Advanced Drug Delivery Reviews 72 (2014) 28–48

Contents lists available at ScienceDirect

Advanced Drug Delivery Reviews

journal homepage: www.elsevier.com/locate/addr

Acoustic behavior of microbubbles and implications for drug delivery ☆

Klazina Kooiman [a,b,1,*], Hendrik J. Vos [a,c,1], Michel Versluis [d], Nico de Jong [a,b,c]

[a] Department of Biomedical Engineering, Thoraxcenter, Erasmus MC, Rotterdam, The Netherlands
[b] Interuniversity Cardiology Institute of the Netherlands (ICIN), Utrecht, The Netherlands
[c] Laboratory of Acoustical Wavefield Imaging, Faculty of Applied Sciences, Delft University of Technology, Delft, The Netherlands
[d] Physics of Fluids Group, MIRA Institute of Biomedical Technology and Technical Medicine, University of Twente, Enschede, The Netherlands

ARTICLE INFO

Available online 23 March 2014

Keywords:
Ultrasound contrast agent
Acoustic cavitation
Acoustic microstreaming
Microcapsule
Co-administration
Drug uptake
Drug carrier system
Drug release

ABSTRACT

Ultrasound contrast agents are valuable in diagnostic ultrasound imaging, and they increasingly show potential for drug delivery. This review focuses on the acoustic behavior of flexible-coated microbubbles and rigid-coated microcapsules and their contribution to enhanced drug delivery. Phenomena relevant to drug delivery, such as non-spherical oscillations, shear stress, microstreaming, and jetting will be reviewed from both a theoretical and experimental perspective. Further, the two systems for drug delivery, co-administration and the microbubble as drug carrier system, are reviewed in relation to the microbubble behavior. Finally, future prospects are discussed that need to be addressed for ultrasound contrast agents to move from a pre-clinical tool into a clinical setting.

Contents

Abbreviations: AALs, acoustically active lipospheres; $[Ca^{2+}]_i$, intracellular calcium ions; HUVEC, human umbilical vein endothelial cells; MI, mechanical index; PEG, polyethylene glycol; PRF, pulse repetition frequency; ROS, reactive oxygen species; P_, peak negative pressure; PI, propidium Iodide.

☆ This review is part of the *Advanced Drug Delivery Reviews* theme issue on "Ultrasound triggered drug delivery".

* Corresponding author at: Erasmus MC, Thoraxcenter, Department of Biomedical Engineering, Room Ee2302, P.O. Box 2040, 3000 CA, Rotterdam, The Netherlands. Tel.: +31 10 70 44036; fax: +31 10 70 44720.
E-mail address: k.kooiman@erasmusmc.nl (K. Kooiman).

[1] Equal contribution of first two authors.

http://dx.doi.org/10.1016/j.addr.2014.03.003
0169-409X/

1. Introduction

In 1968 it was discovered that following saline injection, small echogenic gas pockets were formed, thereby dramatically improving the contrast in the ultrasound imaging [1]. Since then, the gas pockets have evolved into clinically approved ultrasound contrast agents for diagnostic ultrasound imaging [2–8]. More recently, ultrasound contrast agents have been introduced as ultrasound-triggered agents for drug delivery and therapy [9–13]. The reader is referred to various reviews written about the use and different formulations of ultrasound contrast agents. [2–8,14]. For a recent overview of clinically approved ultrasound contrast agents, see [8] or [15].

Ultrasound contrast agents consist of gas microbubbles dispersed in a solution, and are administered intravenously. To improve stability and corresponding circulation lifetime of the agent in the vascular system, the following adaptations are made to the gas microbubbles. First, the gas bubbles are coated with lipid, polymer, sugar or protein material [8,10,15]. The coating reduces the surface tension, and corresponding capillary pressure which drives the gas into solution. Moreover, it provides a gas diffusion barrier. Secondly, the gas core is composed of a heavy molecular weight inert gas, for example SF_6, C_3F_8, or C_4F_{10}, which improves longevity as a result of its low solubility in the surrounding medium. The typical size of clinically approved microbubbles is between 1 and 10 μm in diameter. Because of their size, the microbubbles are contained within the vasculature and can therefore be considered true blood pool agents [7,16].

Microbubbles oscillate in a driving pressure field, and for imaging purposes, gas compressibility provides echogenicity with an improvement of several orders or magnitude compared to solid particles of the same size [17,18]. The bubble oscillations will set the surrounding fluid into motion. More intense oscillations will set up an acoustic streaming pattern which may assist in the mixing and delivery of co-administered drugs. Even higher amplitudes of oscillations lead to asymmetrical collapse and jet formation, which may further promote delivery of the co-administered drugs or incorporated payload. An even further increase of the driving pressure may lead to the spontaneous formation of vapor and gas cavities, termed cavitation. Key to the formation of such cavitation bubbles is the presence of pre-existing cavitation nuclei. Stabilized contrast microbubbles provide such nuclei. The 'strength' of the acoustic pressure field and the applied frequency is classified through the mechanical index (MI), and related to the stability of the microbubbles. This relation is based upon the early MI definition by Apfel [19] and is defined as $MI = \frac{P_-}{\sqrt{f}}$ with P_- the peak negative pressure of the ultrasound wave (in MPa), and f the center frequency of the ultrasound wave (in MHz). Even though the MI has a dimension, it is reported as a dimensionless number. A value of 1.9 is adopted by the US Food and Drug Administration as the safety limit for clinical ultrasound in the absence of microbubbles, as is based on the formation of cavitation bubble, as per the above. Based on the MI, a classification of microbubble behavior can be given [20]. First, a typical setting for contrast agent imaging (power modulation, pulse inversion, contrast pulsing schemes (CPS)) is an MI between 0.05 and 0.2. At higher MI, between 0.2 and 0.5, destruction of the contrast agent (gas loss, shell material loss, bubble dissolution) causes signal deterioration during a clinical exam. However, it is known that bubbles may sustain stable oscillations during acoustic driving caused by so-called rectified diffusion [17]. This regime is termed the stable cavitation regime. Most of these bubbles dissolve once ultrasound is stopped. An MI of above 0.5 is highly destructive for contrast agents [21]. In this review, the ultrasound settings are typically given in terms of frequency and pressure, which can then be converted to an MI value using the equation above.

Microbubbles need to be close to cells in order to trigger drug delivery. One delivery mechanism for drug uptake by cells is termed sonoporation, where pore formation in the cell membrane is induced through mechanical and fluid mechanical stress of the oscillating and/or collapsing bubbles (see also Section 3). Fig. 1 shows an illustration of the key possible mechanisms. Fig. 1a shows the setting where a microbubble is in contact with an endothelial cell. The microbubble oscillates volumetrically in the stable cavitation regime. In the compression phase of the microbubble (middle picture in Fig. 1a), the microbubble pulls on the cell membrane. Furthermore, the liquid neighboring the bubble-wall interface shears along the cell membrane, as denoted by the arrows. In the expansion phase (bottom picture), the microbubble exerts a normal force on the cell membrane, and the shear motion along the cell membrane is pointed outwards. Thus, the stable cavitation regime implies that the liquid and cell around the microbubble are stretched and sheared at the frequency of the incoming ultrasound wave. Since the microbubble oscillations are mild, the oscillations can be sustained over a long duration, potentially setting up an acoustic streaming pattern as illustrated in Fig. 1b. With increasing

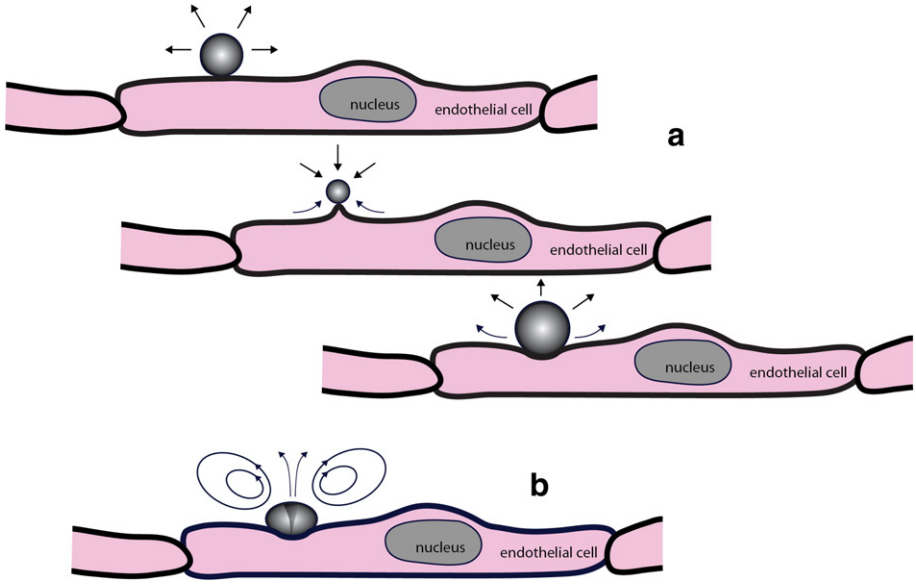

Fig. 1. Illustration of common microbubble phenomena nearby cells. (a) stable cavitation, in which the bubble massages the cell membrane; (b) transient cavitation, in which violent collapses and jets occur, and acoustic microstreaming around the bubble can become significant.

pressure, we also enter the inertial cavitation regime and the bubble will display more violent behavior, such as a collapse, and jetting. Multiple examples will be given in more detail throughout this review. Moreover, we will quantify the order of magnitude of these stresses to facilitate future analyses of stresses exerted by the microbubble on the cell membrane.

Drugs and genes can also be incorporated in the bubble construct. The payload can be contained in the bubble shell, it can be attached to the shell, e.g. in liposomal form, or it can be contained in a thin oil layer in the core of the bubble. Rigidity and drug loading capacity of these types of bubbles is typically improved through the use of a polymeric shell, and we typically refer to these systems as microcapsules [10].

This review will specifically focus on the acoustic behavior of microbubbles for drug delivery. Theory on the relevant concepts of microbubble oscillations will be provided, as well as theory on the interaction of these oscillations with its environment. The two main different drug delivery applications will be covered, namely using microbubbles for co-administration and as drug carrier system. Both flexible coatings and rigid coatings will be evaluated because the type of coating strongly correlates to the acoustical response of the microbubble.

2. Acoustic behavior of microbubbles

2.1. Theoretical microbubble behavior

In this section, we will present the basic equations for gas microbubbles. For encapsulated gas bubbles in a complex surrounding with tissue, red blood cells, and flow, these equations provide an order of magnitude estimate for the normal and shear stresses exerted on a nearby cell layer. Moreover, the equations and resulting graphs show the critical influence of microbubble resonance on these stresses, which is very often neglected in the analysis of drug delivery experiments. By neglecting the resonant behavior, it is implicitly assumed that every bubble is equally effective in drug delivery. We show that based on first principles, it is evident that resonance effects are crucial for stimulating drug delivery.

From first principles, the motion of a spherical gas bubble in a liquid can be described by combining Bernoulli's equation and the continuity equation. This was first described by Lord Rayleigh [22]. Later, the theory was refined by various authors [23–26] to account for surface tension and viscosity of the liquid. The relation between radial motion and pressure difference at the liquid–gas interface (see, e.g., [17] Eq. 3.119 or [27]) is written as

$$\rho\left(\frac{3}{2}\dot{R}^2 + R\ddot{R}\right) = p_{\text{int}} - p_{\text{ext}} \tag{1}$$

where ρ is the density of the surrounding liquid, R is the time-dependent radius of the bubble, $\dot{R}$ and $\ddot{R}$ are the velocity and the acceleration of the bubble wall, respectively, p_{int} is the internal pressure, which includes gas pressure and capillary pressure and p_{ext} the external pressure, which is the sum of the ambient pressure P_0 and the acoustic driving pressure P_a.

The bubble dynamics equation is a nonlinear ordinary differential equation and its solution is a nonlinear relation between the driving acoustic pressure P_a and the radial oscillation R. While the solution can be calculated from a numerical computation, it is instructive to solve the equation in an analytical way through a linearization of the equation. The oscillating radius R is viewed as a small variation $x(t) \ll 1$ around its equilibrium radius: [17,28]

$$R = R_0(1 + x). \tag{2}$$

By inserting this value into Eq. (1), assuming an external driving field $|P_a|$ sin ωt and neglecting higher-order terms, the system is then described by [28]:

$$\ddot{x} + \omega_0\delta\dot{x} + \omega_0^2 x = \frac{P_a}{\rho R_0^2} \tag{3}$$

with $\omega_0 = 2\pi f_0$, f_0 the eigenfrequency of the system and δ the dimensionless damping coefficient. This equation describes a damped harmonic oscillator: the compressible gas acts as a spring, while the displaced liquid around the vibrating bubble acts as the mass. Viscous losses, energy re-radiation, and thermal losses provide the damping of this system. The calculation of the damping and eigenfrequency is thoroughly addressed elsewhere [8,17,18,27–33]. A typical value for the damping of gas bubbles in the micrometer size range is 0.1 to 0.2 at resonance [29]. A first estimate of eigenfrequency can be given based on a simple equation developed in an exquisite paper from Minnaert in 1933 [34]. This estimate is given by $f_0 = \frac{1}{2\pi}\sqrt{\frac{3\kappa P_0}{\rho R_0^2}}$, with κ the polytrophic exponent of the gas inside the bubble. Inserting $\kappa = 1.1$ (for heavy gas like C_3F_8 or SF_6), $\rho = 1000$ kg/m^3, and $P_0 = 100$ kPa, the estimated bubble resonance is generalized to $f_0 R_0 \approx 3$ μm MHz. This value has been proven a good estimator for the relation between frequency and size even for flexible-coated microbubbles.

Assuming a steady-state response ($t \to \infty$) and combining Eq. (2) and Eq. (3) gives the relative amplitude of oscillation:

$$|x| = \frac{F_0}{\sqrt{\left(\omega_0^2 - \omega^2\right)^2 + (\delta\omega\omega_0)^2}}. \tag{4}$$

In this equation, $F_0 = \frac{|P_a|}{\rho R_0^2}$ with $|P_a|$ the amplitude of the driving acoustic field. Fig. 2 shows a graphical representation of the amplitude as a function of the driving frequency, the so-called resonance curve. When the bubble is excited at its eigenfrequency ($\omega = \omega_0$), then the relative amplitude is determined by the ratio of driving force F_0 and the damping term. When excited at a lower or higher frequency, the amplitude of oscillation decreases. The linear resonance frequency of the system is defined by the frequency at which the radial excursion is maximal, which is near (but not equal to) its eigenfrequency. The resonance frequency can be derived from the previous equation by setting $\mathrm{d}|x|/\mathrm{d}\omega = 0$, yielding:

$$f_{\text{res}} = f_0\sqrt{1 - \frac{\delta^2}{2}} \tag{5}$$

The relation between resonance frequency and size is plotted in Fig. 2b.

As seen from the first principles above, microbubbles resonate and have a frequency of maximum radial response to the driving ultrasound field. This maximum radial response, in turn, has several implications on the efficacy of drug delivery when the bubble is excited near resonance. It implies:

- A maximum interaction with cells;
- A maximum streaming potential, and consequently, a maximum shear stress;
- A maximum release of drugs when they are incorporated in the bubble construct;
- A maximum mixing of the bubble surrounding introducing fresh sample from the medium into the region of interest.

This is the reason why acoustic triggering of bubble-mediated drug delivery is mostly done using diagnostic ultrasound frequencies: for flexible-coated microbubbles ranging 1–10 μm in diameter, the resonance frequency lies within the range of frequencies (1–10 MHz) used for medical ultrasound imaging from outside the body [17,35]. In case

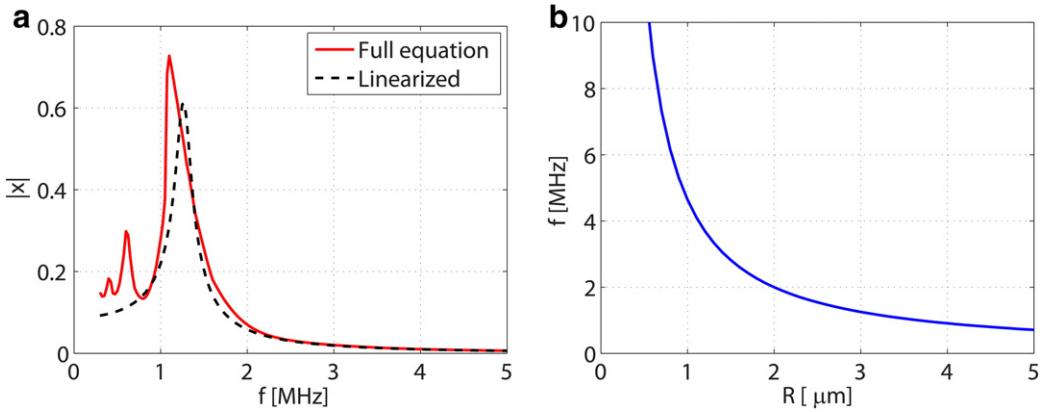

Fig. 2. (a) Radial excursion versus frequency of an uncoated air bubble, based on Eqs. (5) (Linearized) and the modified Rayleigh–Plesset equation (full equation) [8]. The radius is 3 μm, driving pressure amplitude 50 kPa, damping coefficient is 0.14. (b) Resonance frequency versus radius.

of a polydisperse population of microbubbles, there is not one single resonance frequency, which means that only a subset of microbubbles will resonate to the driving frequency. The other microbubbles will be excited, but they will have a lower radial excursion than can be expected from resonant microbubbles, and will primarily contribute to attenuation of the acoustic waves instead of contributing to drug delivery. A circumventing approach would be the use of frequency sweep signals, also called chirps, to activate a larger subset of microbubbles at resonance. McLaughlan et al. [36] very recently reported on this approach.

The full non-linear solution of the bubble dynamics is commonly described by the so-called Rayleigh–Plesset equation, see e.g. refs [8,17,29,33,37,38]. The result of solving the modified Rayleigh–Plesset equation [8] for a gas bubble of 3 μm radius is also shown in Fig. 2a. The resonance curve changes shape compared to the linearized solution, and several secondary resonance peaks are visible at the lower frequencies. These are indicative of nonlinear responses. However, overall the amplitude of oscillation appears to be very similar. This similarity suggests that the use of linearized equations suffices to describe the microbubble behavior with reasonable accuracy for drug delivery in case of stable cavitation. In case of inertial cavitation, when the radial oscillation amplitudes exceed the Blake threshold $R_{max} > 2.2R_0$ [17] the linearized equations fail to describe the phenomena and the full non-linear equation must be solved [17,27]. Microbubbles oscillating in this regime can even produce shock waves.

2.2. Coating

To stabilize the bubbles and to prevent their coalescence or dissolution in the circulation the bubbles are coated with a stabilizing layer. Drug delivery systems also incorporate drugs onto or in the coating. The coating changes the bubble dynamics. Typically, there are two types of coatings, flexible coatings of phospholipids and solid encapsulations of e.g. polymers. The phospholipid coating has a thickness of a few nanometers (monolayer), the rigid coating is typically of a thickness of tens of nanometers.

To account for the coating of diagnostic and therapeutic microbubbles, many authors have proposed modeling the shell rheology by viscous [39], viscoelastic [38–40], shear-thinning [30,31,33], or viscoelastic thin film [41] effects, as extension to Rayleigh–Plesset based equations. Refs. [8,42,43] summarize the various models presented earlier. Despite the numerous papers, no consensus exists on the best model to describe the details of the phenomena observed for microbubbles [8]. One reason for this is that bubbles of exactly equal size and type do have dispersion in their response [30,44–46], possibly caused by inherent structural organization in the coating [47]. The elastic coating of the phospholipids increases the resonance frequency, up to a factor 40%, which is confirmed by experiments [30,48]. The viscous coating also increases the damping by up to a factor 5. Nonetheless, inertial effects dominate the microbubble behavior, rather than coating rheology, for pressure ranges relevant to drug delivery applications [49,50]. Therefore, the behavior of gas bubbles presented above is most relevant for flexibly coated microbubbles.

In case of a rigid coating, the oscillatory dynamics are dictated by the capsule properties. This results in much higher resonance frequencies [51]. However, it has been shown that the gas bubble formed after rupture of the capsule is most relevant for the subsequent biological effects (see Section 4.2). This supports that the relevant physical behavior can be described in terms of free gas bubbles.

2.3. Radiation force

Oscillating microbubbles can translate in a medium, through the so-called radiation force [17,27]. In case of a traveling acoustic wave, the bubbles translate in the direction of wave propagation. In case of a standing acoustic wave, the bubbles translate to nodes or anti-nodes of the acoustic field, depending on the phase difference between the bubble volumetric oscillation and the pressure wavefield. For details, the reader is referred to the large amount of literature, e.g., Refs. [17,27,46,52,53]. The velocity of a freely floating microbubble can reach values up to order of meters per second in case of resonant microbubbles in water [46,53], compensated by the duty cycle of the pulses. For example, in case of 10% duty cycle, the bubble average velocity can reach up to 0.1 m/s, which can compete with regular blood flows in medium and small-sized vessels.

The radiation force is called the *primary* Bjerknes force after [52] when it is a resulting force of the incident acoustic wave. The force is called *secondary* Bjerknes force when it is a result of a nearby bubble driven by the same field. In this case the oscillating microbubble acts as a secondary ultrasound source. The acoustic radiation force can lead to three effects that are relevant for drug delivery:

- A microbubble in a regular medical ultrasound field will be pushed in a direction away from the probe, towards the distal wall [46];
- A microbubble near a rigid wall will experience a net attractive force towards the wall, due to the secondary radiation force caused by its image bubble [54,55];
- Microbubbles that are within a distance of a few radii from each other tend to cluster because of the attractive secondary Bjerknes force. Bubble coalescence as well as bubble fission can occur within the cluster [49,56]

The net result of the above effects on the drug delivery cannot be given a-priori. The first effect will increase the chance of bubble contact to the distal wall, but it will decrease the chance of contact between bubble and proximal wall. The second effect will increase the contact

force between the bubble and the wall, but the magnitude of the force may be small compared to the drag force in the flow of the vessels, or to the primary radiation force. The third effect may result in larger bubbles, with a consequently lower resonance frequency and increased lifetime. The cluster dynamics can be described by the same bubble dynamics equation using the cluster radius as an effective input radius of the system, which therefore also resonates at a lower driving frequency (see note by [57]). Clustering effects have been observed in vitro, but the in vivo concentration of microbubbles may be too low to have 'a distance of a few radii' between the bubbles on average.

2.4. Experimental methods

In early years, microbubbles for medical applications were characterized by the acoustical scattering and attenuation properties of a population of bubbles [40,58]. Acoustic ensemble-averaged characterization is relatively inexpensive and has the advantage of a high sampling rate. However, it is very difficult to relate the ensemble-averaged behavior to single microbubble dynamics, or even to a subset of microbubbles of similar size. Acoustic experiments on single microbubbles have also been carried out, but the scattered pressure of a single bubble is limited (order 1 to 10 Pa) which is close to the noise level of any acoustic detection system. To isolate single microbubbles, the concentration should be much smaller than an order of one bubble per mm^3, which is dictated by the transducer focal region, and the size of the microbubble at hand should be measured independently. This has resulted in only few single microbubble acoustical studies [59–61], which however could confirm the optically observed relations between microbubble size and acoustic behavior.

Advances in optical experimental technology gradually provided means for studying individual bubble dynamics. One method exploits laser-light scattering [43], which gives a relative value of the instantaneous 1-dimensional (1D) size. Other methods rely on ultra high-speed microscopy. A typical setup with a microscope includes an optically and acoustically transparent wall, to which microbubbles float up by buoyancy. In addition this allows for precise focusing of the optical equipment. The application demands that a camera should be able to temporally resolve the dynamics of the microbubbles driven at MHz frequencies. The required frame rates makes the construction of such a camera expensive, and the recording time is limited by the number of frames. In 1999, bubble dynamics were resolved in a 1D streak image using a microscope and camera setup [32]. In addition, the camera used (Imacon 468) could also store seven 2D frames at high frame rate, facilitating the interpretation of the streak images. Higher frame numbers were available in the Ultranac system (twenty-four 2D frames) [62], and in the Brandaris 128 camera system, which is able to record 128 frames at rates up to 25 million frames per second (Mfps) [63].

Recently, the Brandaris-128 camera was extended with fluorescent imaging capability. Despite the relatively low fluorescent signal compared to bright field imaging, the system is capable to resolve molecular pathways by specific fluorescent binding [64]. Chen et al. [65] report on the development of a Brandaris-128-type camera, but redesigned for higher fluorescence sensitivity, leading to higher frame rates for fluorescence imaging. It is expected that ultrahigh speed fluorescent imaging will further improve the understanding of drug delivery dynamics.

2.5. Flexible coating

The observations obtained for coated bubble are different for flexible and rigid coatings. This section describes the flexible coatings, while the next describes rigid coatings. Phospholipids-coated microbubbles are spherical at rest because of surface tension. Nonetheless, the lipid coating may be inhomogeneous by nature, which may lead to imperfect spherical shapes retaining internal stresses [66].

Microbubbles with a flexible coating such as phospholipids show various oscillation regimes, characterized by their volumetric oscillation dynamics, and shape. They can be listed in order of increasing volumetric oscillation amplitude: (I) no oscillation; (II) linear spherical oscillations; (III) nonlinear spherical oscillations; (IV) non-spherical oscillations; (V) violent inertial collapses; and (VI) bubble fragmentation/fission. These will be described in detail in the following.

Emmer et al. [67] showed that phospholipid-coated microbubbles have a threshold for linear oscillation when driven at relatively low pressure amplitudes (30–120 kPa at 1.7 MHz). The cause for this strongly non-linear effect was found through theoretical considerations in Refs. [41,68]. The phospholipids coating is considered as a viscoelastic film that buckles in the bubble compression phase, stretches in the equilibrium state with elastic behavior, and breaks up in the expansion phase [41]. These non-linear effects are most pronounced at low acoustic pressures, and therefore most visible at low-MI experiments (MI < 0.1). Since drug delivery in general uses larger MI values, the threshold effect may not be directly relevant for regular drug delivery. Yet, the effect is highly relevant for contrast *detection* modes on clinical echo machines.

Various studies address a pressure regime in which the response of microbubbles is relatively linear to the driving pressure [30,37,69]. Linearity was often assumed to match the various bubble parameters in theoretical models to the observed microbubble dynamics. However, the validity of such indirect methods depends on two factors: (I) the applicability of the bubble dynamics model, and (II) the inter-dependency of the model parameters on the microbubble behavior. For example, in [37] the shell thickness and shell viscosity was fixed and it was found that the shell elasticity increases with increasing bubble radius. The experiments were performed with a single applied frequency (0.5 MHz) and pressure (40–80 kPa). Van der Meer et al. [30] insonified single microbubbles consecutively with 11 ultrasound pulses of increasing frequency. A best fit between the resulting resonance curve and simulated resonance curves was found by varying both shell elasticity and shell viscosity in the simulation. They found that the shell elasticity was nearly constant while the shell viscosity decreases with decreasing shell dilatation rate ($\dot{R}/R$). This example shows that the results of fitting methods are only predictive in conjunction with the specific model used, and in similar experimental conditions. Nonetheless, the experimentally obtained curves are predictive for interactive forces between bubbles and cells, as will be described later in this review.

The oscillations of microbubbles show many nonlinear effects. These include the generation of higher harmonic frequencies of the driving frequency [17,70], period-doubling [71–73], and frequency-mixing [44]. These effects can occur for both coated and free microbubbles. Phospholipid-coated microbubbles, in addition, can also show *compression-only* behavior, in which the compressional half-cycle has much larger amplitude than the expansion half-cycle [41,74]. Although these effects are very beneficial for discriminating microbubble signals from tissue signals, and hence for their imaging, the influence on drug delivery of these nonlinear effects is presumed limited. Another conclusion can be drawn from the past 10 years of in vitro measurements. Microbubbles in relevant clinical conditions never show pure linear behavior: At small radial excursions, the nonlinear behavior of the coating dominates the oscillation [68]. At larger radial excursions, the intrinsic nonlinear behavior of gas bubbles (as expressed in the Rayleigh–Plesset type equations) dominates the oscillation. No intermediate region is present.

The microbubble surface can show non-spherical shape oscillations in conjunction with the regular volumetric oscillations. The causes can be multiple. First, parametric instabilities of the surface can occur. These need tens of cycles of a tone bursts to build up [75]. Vibrating bubbles close to or in contact with a wall can also show non-spherical shapes oriented perpendicularly to the wall [76–79]. Vos et al. [55] systematically studied the microbubble oscillations in contact with a wall from two directions, thus allowing for analysis of both a top-view and

a side-view. Because of the presumed high relevance of such oscillations to drug delivery, the shape oscillation in presence of a wall is described in more detail below.

Fig. 3 shows a sequence of recorded images [80] from a 9 μm bubble insonified with a tone burst of 6 cycles at a frequency of 1 MHz and an amplitude of 140 kPa. In top view (top panel of Fig. 3), the bubble shows a circular shape throughout, without deformation. When viewed from the side (bottom panel) the bubble shows alternatingly prolate (defined by having two short axes and one long axis) and oblate shapes (two long orthogonal axes and one short). In frames 4–6, the bubble is even seen to momentarily split. Between frames 9 and 10, the bubble wall velocity in the sequence is one order higher (~70 m/s) than the typical bubble wall velocity during oscillation. The results are in line with [77]. Notably, the center of the microbubble also shows a strong period-doubling behavior: in frames 5–9 it is located further away than in the subsequent expansion phase of the microbubble, frames 11–16. The translation of the center of mass, and its phase delay with respect to its volumetric oscillation, largely dictates the fluid motion around the microbubble [81]. Consequently, the translation will also influence the stresses at the wall. The splitting of the bubble observed in frames 4–6 is followed by re-coalescence in the subsequent frames. On the contrary, it has also been observed that a sub-micron gas bubble was pinched off from the mother bubble [55,82]. The pinched-off submicron gas bubble survived for over 80 ms, indicating that the surface was covered with a phospholipid coating. As the pinched-off bubble was formed on the opposite side of the wall, a traditional 'top view' would not be able to reveal the occurrence of pinch off. Frames 11–16 in Fig. 3 show a jetting phenomenon inside the bubble, in which a tiny jet of liquid hammers the wall. The velocity of the tip of a jet can become 100 m/s in such circumstances ([27] Eq. 3.9, with $\Delta p = 150$ kPa, $\xi = 8.6$, $\rho = 1000$ kg/m^3), introducing a concentrated force on the wall. Vos et al. [55] have shown that jets are observed regularly for resonant microbubbles insonified at a frequency of 2.25 MHz and a pressure between 150 kPa and 300 kPa (M.I. of 0.1–0.2). Note that this is a range of pressures that is very commonly used in microbubble-mediated drug delivery application. Therefore, it is very likely that jetting phenomena play an important role in sonoporation.

Violent collapses of microbubbles occur when the oscillation amplitude becomes very large [56,79,83]. A symmetrical collapse focuses the available energy into a fraction of the original bubble volume, leading to an enormous pressure increase and temperature rise [84,85]. The bubble collapse leads to the emission of a shock wave, a mechanism that is even used by the pistol shrimp to stun small fish [86]. The effects of such a violent collapse near a cell layer vary from membrane opening to hemorrhage. These are addressed elsewhere in this Journal issue. It should be noted here that such violent collapses lead to broadband ultrasound emission, which can be detected experimentally [19,27,87,88].

The microbubble can be broken up in several smaller microbubbles, in rebound of a violent collapse [56,83]. Such fragmentation was observed when $R_{max}/R_{min} > 10$, which is a stability criterion developed by Plesset and Mitchell [89]. Fragmentation has been observed in vitro at MI = 0.2 (at 2.25 MHz) for diagnostically-relevant pulses [90], although it should be noted that the fragmentation in vivo appears only at larger pressure values [49].

2.6. Rigid coating

Polymer coatings are very rigid and this increases the resonance frequency to >15 MHz [51] for capsules of a size of 3 μm. Because of the dominant role of the encapsulation, microcapsules have three oscillation regimes: no oscillation, small non-spherical oscillations, and sonic cracking followed by gas release and violent gas collapse. High-speed recordings will be shown below to illustrate this behavior [51]. Fig. 4 shows optical recordings of a microcapsule driven at low MI (f = 1 MHz; MI = 0.24). The mixed gas/oil-filled polymeric microcapsules typically compressed without shell cracking. An area–time

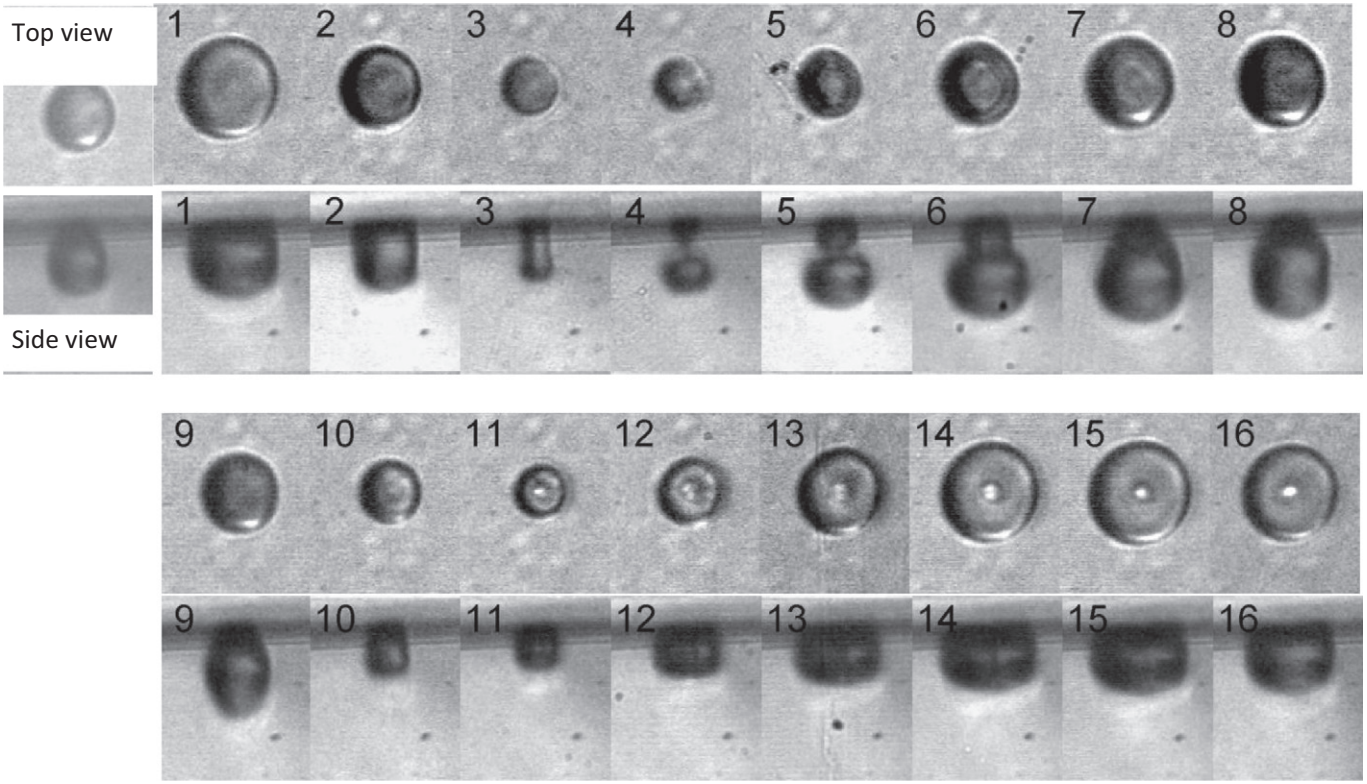

Fig. 3. Optical images of the bubble during 2 cycles of the ultrasound pulse. Top panels show top view images at an interframe time of 138 ns. The bottom panels show the same segment of bubble oscillations in side view, recorded 2 min later. The bubble wall appears as a gray region on the top. Resting diameter of the bubble (left) was 9 μm. Ultrasound parameters were 1 MHz, 140 kPa peak negative pressure.

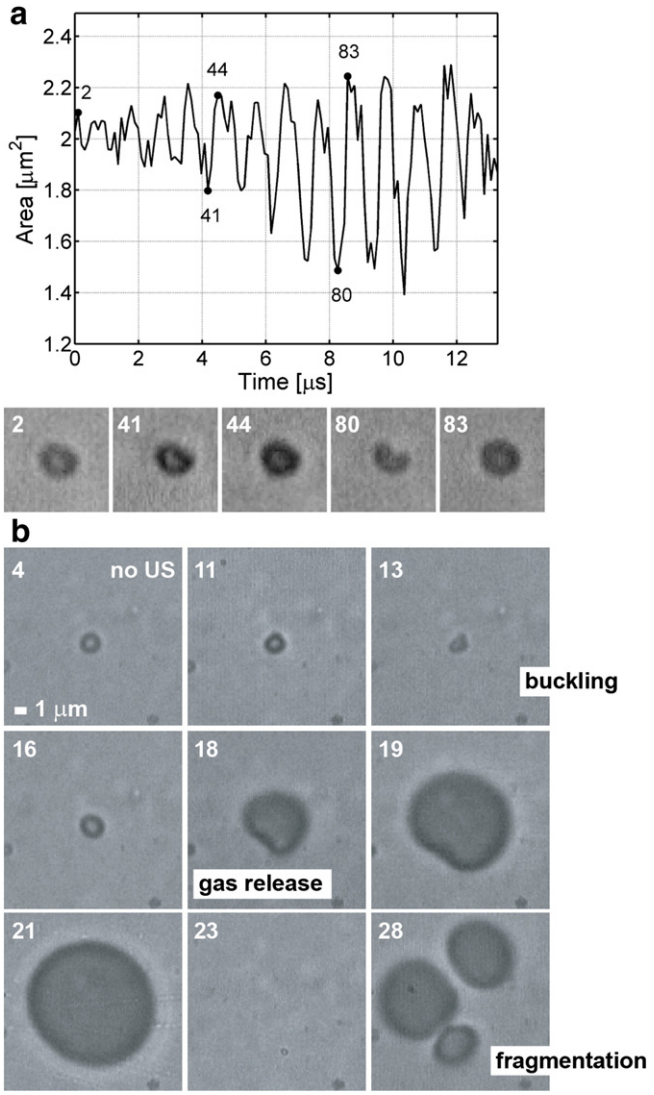

Fig. 4. Brandaris 128 high-speed camera recordings of microcapsules with high oil fraction and low gas (11 ± 1%) fraction insonified at 1 MHz. Frame rate is about 9.5 million frames per second. A) Recording of a microcapsule of 1.6 μm in diameter, insonified at P_ 0.24 MPa (MI = 0.24). Top panel: Area–time curve. Bottom panel: five selected cropped frames (4.5 by 4.5 μm) showing the microcapsule before insonification (frame 2) and during insonification (frame 41, 44, 80, and 83). Compression but no cracking is observed. B) Recording of a microcapsule of 1.8 μm in diameter, insonified at *P*_ of 0.51 MHz (MI = 0.51). Gas release is observed.
Reprinted from [51].

curve of a recording of a microcapsule is given in Fig. 4A (top panel). During insonification, the microcapsule compresses but hardly expands. The compression shape was non-spherical, but rather buckled on one side. Buckling behavior was more pronounced later in the US burst than in the beginning of the US burst, showing increasing weakening of the encapsulation during the insonification.

When insonified at a higher MI ($f = 1$ MHz; MI = 0.51), microcapsules typically buckled only once, leading to cracking of the encapsulation. The weakest spot in the shell is most likely to buckle. In the following negative pressure half-cycle of the acoustic pulse, gas escape was observed. Fig. 4B illustrates this effect. The microcapsule buckled (frame 11–13) and returned to its original spherical shape (frame 16). This was followed by gas escaping from the microcapsule (frame 18–21). In frame 23, the free gas was compressed to such an extent that it was no longer visible. In the subsequent expansion phase, the gas expanded again into three free gas bubbles (frame 28). During the following US cycles, the free gas bubbles continued to expand, collapse, and coalesce. The free gas bubbles were no longer visible in a successive recording that was taken 80 ms later, indicating that they had dissolved. This can be expected from uncoated gas bubbles of micrometer size range [91]] [Note that uncoated gas bubble may survive for 80 ms when they are acoustically excited with continuous waves. This effect is called rectified diffusion [17]. However, in this experiment the bubbles were not excited in the 80 ms time interval, hence our expectation that they are likely to dissolve]. This example shows that the gas bubble violently oscillates after capsule cracking, caused by the high MI that is needed to induce the cracking. The gas bubbles in this pressure regime will show equal effects as the phospholipids-coated microbubbles such as collapse, jetting, and fragmentation.

The buckling and rupture behavior observed for the microcapsules is well predicted by Marmottant et al. [92]. They calculated the stresses in the shell during insonification, and show that thin solid shells (such as that of the albumin-coated contrast agent Albunex and the microcapsules described above) first buckle before they rupture, while thick shells only rupture. The model was experimentally verified by Lensen et al. [93] by systematically varying the ratio between shell thickness and diameter. Depending on the ratio of shell thickness and ratio, rupture pressures of 0.3 to 1 MPa were found at a driving frequence of 1 MHz. This is consistent with the pressure threshold values for ruptue of microcapsules found in other studies [51,90,94]. See also Fig. 5 for an acoustic event count, i.e., rupture, of populations of polymer-coated microcapsules, which correlates well with the rupture pressures stated before. The results by Lensen et al. [93] show that the pressure threshold for rupture can be accurately predicted and controlled. This is an important result for co-administration of drugs, since it implies an even better control on the activation location of the microbubbles.

2.7. Interactions of microbubbles with their environment

To accurately model the behavior of microbubbles in tissue, various effects need to be accounted for. First, the no-slip condition of fluid motion at the vessel wall leads to a viscous boundary layer nearby the wall that adds damping to the bubble oscillation. Second, tissue is an elastic soft solid, as opposed to rigid walls which are favored in in vitro setups and modeling. Third, capillaries and arterioles confine the bubble oscillations. Fourth, the bubble shows non-spherical shape oscillations. Fifth, blood is a non-Newtonian fluid. Sixth, temperature may change the coating's properties. All these effects will strongly affect the modeling accuracy. In the next subsection we summarize the simplest method to address a stiff wall neighboring the microbubble. Moreover, we summarize studies that address the boundary conditions of microbubble oscillations in vivo.

There are basically three routes through which a microbubble is forcing on neighboring tissue. The first is a mechanical 'palpation', which forces normally to the cell membrane, in alternating direction

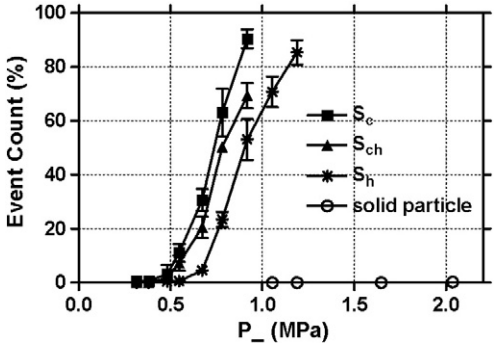

Fig. 5. Acoustic event count of rupture of microcapsules as function of acoustic pressure. Frequency 1 MHz, 32 cycles. S_c = air-filled microcapsules, S_{ch} = mixed oil/gas (39 ± 1%) filled microcapsules, S_h = oil filled with a small fraction of gas (11 ± 1%) in microcapsules.
Reprinted from [51].

[55,95]. The second is a shear stress caused by the fluid that shears along the cell membrane, caused by the oscillating microbubble. The third is a jetting phenomenon.

Going further on the linearized equations of motion, it is possible to calculate the normal and shear stresses that are exerted by a microbubble at the neighboring wall. Let us start with the normal stresses, that correspond to the situation illustrated in Fig. 1.

Using Eq. (1), $x(t) = \varepsilon \sin(\omega t)$, and $0 < \varepsilon \ll 1$, this equation can be linearized to

$$p_L = \rho \varepsilon R_0^2 \omega^2 \tag{6}$$

[Note that even if $\varepsilon = 0.5$, the linearization produced only 20% lower normal stresses compared to the full equation, and thus predicts the magnitude quite accurately]. When inserting regular values for stable cavitation, $\rho = 10^3$ kg/m^3, $\varepsilon = 0.5$ (corresponding to the situation depicted in Fig. 6, driving pressure = 50 kPa), $R_0 = 3$ μm, $\omega = 2\pi\ 10^6$ rad/s, the normal stress is around 180 kPa. This value seems extraordinary large compared to a driving pressure of 50 kPa. The explanation of the larger normal stress nearby a bubble is found in its resonant nature, which means that acoustic energy is focused in the oscillation. This factor alone again stresses the importance of the resonant nature of bubbles for drug delivery.

Looking further into Eq. (6), the normal pressure depends on the product of R_0 and ω. As shown in Section 2.1, this product is relatively constant for resonant microbubbles. Therefore, it is expected that the normal stress is similar for different radii as long as they are excited at resonance. Fig. 6a plots the normal stress as function of driving frequency for microbubbles of 1.5 μm radius or 3 μm radius. All other parameters are equal to those in Fig. 2. It indeed shows that the maximum normal stress is generated at resonance, and has similar values, around 300 kPa. This is around 6 times larger than the incident pressure wave, again showing the large effect of energy focusing on the pressures generated in the liquid near an oscillating microbubble. In case of a collapsing microbubble (inertial cavitation), $\dot{R}$ and R in Eq. (1) can become very large in magnitude, which means that also the normal stresses become very large. A violent collapse can easily generate megaPascals of pressure [17,27].

In case of coated microbubbles at a rigid wall, the damping of the microbubbles is larger than that of free gas bubbles. Moreover, non-spherical oscillations will occur. Nevertheless, even in such circumstances, the normal stress are calculated to become 2 to 5 times larger than the driving pressure in case of stable cavitation [55]; Fig. 12]. The palpation effect by violent collapses can even lead to destruction of capillaries [50], which is, strictly speaking, a regime beyond drug delivery.

An oscillating bubble near a wall produces shear stresses on the wall. The shear stresses evolve from two phenomena, which are the periodic 'AC' motion of the fluid at the oscillation frequency (see Fig. 1a), and a 'DC' motion of the fluid also known as microstreaming (see Fig. 1b).

The order of magnitude of the shear stress caused by the 'AC' motion can be derived as follows. The shear stress on the wall τ_w is generally calculated by

$$\tau_w = \eta \left. \frac{dU}{dz} \right|_{z=0}, \tag{7}$$

assuming a Newtonian fluid in laminar flow. In this equation, η is the dynamic viscosity of the liquid, U the fluid velocity in a direction parallel to the wall, and z the distance variable ($z = 0$ at the wall). For simplicity of the analysis, we assume a no-slip boundary condition at the wall ($U_{z=0} = 0$), and approximate the derivative with the ratio $\Delta U/\Delta z$. The peak velocity of the fluid near the wall and microbubble is on the same order of magnitude as the velocity of the bubble wall itself, expressed by $\Delta U = O(2\pi f \varepsilon R_0)$. The effective distance Δz is provided by the viscous boundary layer [9,96], defined by

$$\Delta z = \sqrt{\frac{\eta}{\pi f \rho}}. \tag{8}$$

Combining the relations above, the order of magnitude of 'AC' shear stress is calculated as

$$\tau_w = O\left(2\pi f\ \varepsilon R_0 \sqrt{\pi \eta f \rho}\right). \tag{9}$$

Inserting the values of a resonant microbubble of 3 μm, $f = 1.2$ MHz, $\varepsilon = 0.5$, and assuming $\eta = 10^{-3}$ Pa s (water), the shear stress is on the order of 20 kPa. For comparison, Vos et al. [55] calculated that the value of the 'AC' shear stress at the oscillation frequency can reach up to 75 kPa for non-jetting bubbles oscillating non-spherically, showing good agreement in order of magnitude. Blood only has a few times higher viscosity compared to water, and thus the shear stresses in blood will be of similar order of magnitude.

The microstreaming field, or 'DC' motion field, is determined by the microbubble dynamics, i.e., its oscillation frequency, but also its oscillation shapes, and by the viscosity and density of the surrounding liquid [71,97]. The presence of such microstreaming patterns around clinically-relevant microbubbles has been shown by few groups [64,81,98] using fluorescently labeled vesicles. Fig. 7 shows the microstreaming pattern around an oscillating microbubble [99], obtained with high-frame rate fluorescence imaging. The flow around the microbubble enhances mixing of the fluid near the microbubble, which may increase drug delivery efficacy; however, a direct relation between fluid motion and drug delivery has yet to be established.

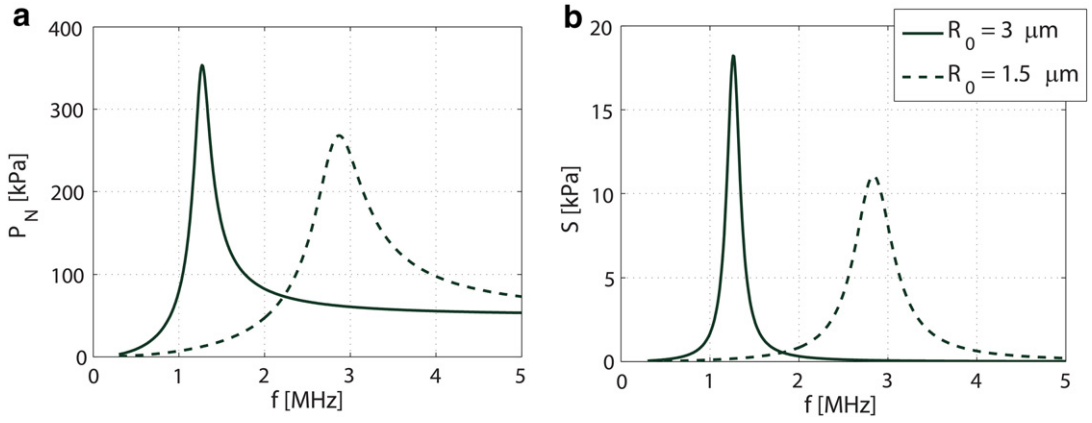

Fig. 6. (a) Calculated normal stress in the liquid just outside of the oscillating microbubble; (b) calculated shear stresses at a nearby wall, caused by acoustic microstreaming. Simulation parameters are equal to those in Fig. 2.

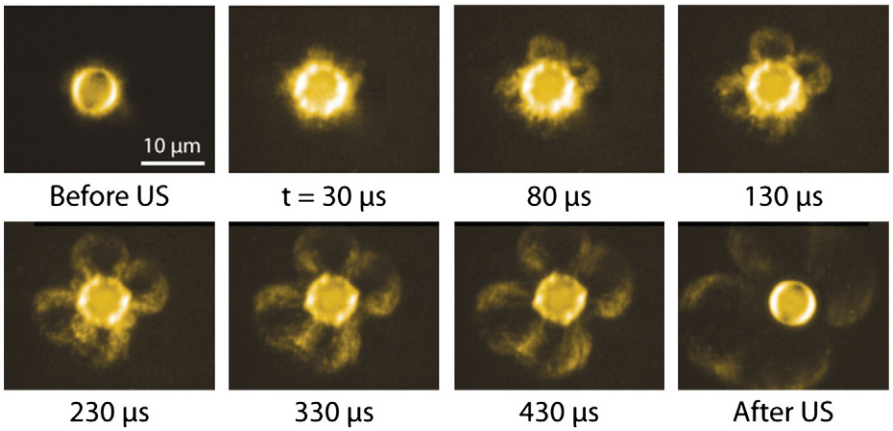

Fig. 7. Fluorescence high-frame rate recording of microstreaming around a liposome-loaded microbubble showing a mode oscillation. Excitation was a 1-Mhz tone burst of 80 kPa, 1000 cycles.
[reprinted from [99]]

The shear stress on a wall caused by the 'DC' microstreaming can be estimated by [9,96]:

$$S = \frac{2\pi(\varepsilon R_0)^2\sqrt{\pi\rho f^3\eta}}{R_0}. \quad (10)$$

The predicted stress values for an air-filled microbubble are plotted in Fig. 6b. It shows that the predicted shear stress values can reach 10 to 20 kPa, and are highest at the resonance frequency by which ε is largest. Note that this shear stress is uni-directional, and is sustained during the entire pulse duration, which make it act on a micro-second time scale, as opposed to the AC shear stresses that act on a nano-second time scale.

The range of shear stresses calculated above have also been found in a hybrid theoretical/experimental analysis on microbubbles [55,100]. Other studies report lower values, e.g., [101,102] report shear stress values of order 1 kPa. Dijkink directly measured shear stresses of up to few kPa originating from the spreading of fluid after jet impact [103]. The reported values for shear stress are larger than regular shear stress values in healthy vessels caused by blood flow, which is 0.1–7 Pa [104]. Moreover, 12 Pa was the value reported for the onset of drug uptake by Wu et al. [102], while Rooney [96] reports higher values for the critical shear stress for hemolysis, 0.3 kPa to 4 kPa. Moreover, he also suggests that the 'DC' contribution has largest impact on the sonoporation. Nevertheless, for both the DC and AC components of the shear stress, it remains to be seen how the difference in time scale will affect biological phenomena.

Both the pinching force and the shear stresses associated with jets can become very large [105]. In an order of magnitude calculation, the stagnation pressure caused by a jet is given by

$$p_{\text{jet}} = \frac{1}{2}\rho U_{\text{jet}}^2. \quad (11)$$

Inserting the reported value above for the jet velocity of 100 m/s, the stagnation pressure can reach values of several megaPascals. As important, the direction of the jet depends on the elasticity of the nearby wall. In a systematic study, [106] show experimentally that the jet points towards the wall if the elastic modulus is on the order of 2 MPa, while in case of an elastic modulus <1 MPa, the jet points away. In general, the elastic modulus of healthy vessels is below 1 MPa, showing that the jet is more likely to point away from the tissue. This has been experimentally validated by Chen and co-workers [107] in ex vivo rat mesentery. It should be noted that many in vitro drug delivery experiments are performed with monolayers of cells attached to a relatively stiff membrane. The distance between the microbubbles and the membrane is only few microns, which is small enough for acoustic interaction [106], despite the intermediary cell. The stiff membrane will force a jet pointing towards the wall, which is opposite to the in vivo drug delivery situation where the entire environment is soft tissue. Therefore, claims based on tissue-mimicking monolayers of cells on a membrane should be considered with great care.

A wall can influence the oscillation dynamics of microbubbles, see e.g. [48,78,108] for direct experimental proof. In literature several extensions to the bubble dynamics equations have been made to account for a vessel wall near an oscillating microbubble [57,76,109–111]. Doinikov and coworkers [57,109] have theoretically studied the influence of a solid wall, a fluid interface, and a fluid thin layer near an oscillating microbubble although experimental data lacks clear validation of the theoretical predictions near a fluid layer or half-sphere. One rudimentary and traditional method to model the influence of the wall is called the method of images (see, e.g., [17,57]). Both the resonance frequency and the damping are found to decrease in the order of 20% compared to the bubble in free space [48]. Experiments showed 30% of resonance frequency decrease [48], indicating that the method of images produces reasonable results despite its rudimentary approach. Moreover, it has been shown experimentally that adherence of functionalized microbubbles to a wall significantly decreases the oscillation amplitude [48,77], see also Section 3.

Various studies have addressed the confinement caused by capillaries and arterioles [49,111,112]. The confinement leads to significant oscillation amplitude reduction, as verified in vivo in a chicken embryo model [113] and ex vivo in the ilecolic vein of a rat [49]. In [113], the authors suggest that the increased viscosity of blood, compared to water, resulted in this reduction of amplitude. Nevertheless retrospectively, the confinement effect may equally have played a role. Moreover, it has been shown that non-spherical oscillations occur frequently in vessels [49,107,113], which strengthens the hypothesis for confinement effects.

Most in vitro experiments for studying the behavior of microbubbles are performed at room temperature. However, temperature plays an important role in the rheological behavior of phospholipids [47] and, consequently, in the behavior of phospholipid-coated microbubbles [45]. Therefore, great care should be taken when translating microbubble behavior at room temperature in vitro directly to results from in vivo applications. Intrinsically, in vitro drug delivery experiments with living cells demand a temperature-regulated environment, thus matching the temperature of the experiment to in vivo application.

2.8. Conclusion

As was seen in this section, the microbubble behavior is rather well known, except for some detailed behavior in the complex in vivo environment. However, the exact relation between microbubble behavior and dynamics and drug delivery potential is largely unknown. The following sections clarify the known and unknown in this relationship.

3. Co-administration

3.1. Flexible-coated microbubbles

The first article that reported sonoporation using ultrasound and ultrasound contrast agents was by Bao et al. in 1997 [114]. Since then, many more papers have been published ranging from in vitro to preclinical to clinical. Although the clinical case study by Kotopoulis et al. [115] presents interesting results, the observed therapeutic effect in five patients with pancreatic adenocarcinoma is disputable. More controlled studies are needed to confirm the significance of the therapeutic effects at these ultrasound settings (diagnostic ultrasound and SonoVue at a relatively low MI of 0.4, a frame rate of 4 per second and a short transmit pulse). Despite the vast amount of studies, so far the exact mechanism of sonoporation remains under debate, although several hypotheses exist. The microbubble behaviors hypothesized include cavitation, inertial cavitation, jetting of microbubbles, microstreaming induced by vibrating microbubbles themselves, microbubbles penetrating cells, and nano-scale cavitation formation inside the cell membrane. This indicates that drug uptake can be induced through several pathways. On the other hand, different studies show conflicting results as some studies show that inertial cavitation is required for the induction of drug uptake [87,116,117], whilst another [118] shows that cavitation itself is sufficient. Another study shows that standing waves are required for drug uptake [119]. Microbubble jetting has been observed near a cell layer [78], but the effect on drug uptake was not studied. The influence of microstreaming is studied in a limited number of experiments, but there are a few theoretical approaches [102]. A novel hypothesis is that insonified microbubbles can penetrate cells by traveling through the cell membrane, as reported by Delalande et al. [120]. However, the microbubble lipid coating found inside the cell can also be explained by fusion or internalization of coating fragments with the cell. Further experiments are needed to elucidate this process. In addition, the relation with drug delivery has to be established because if microbubbles as a whole penetrate cells, they are likely to induce large pores in the cell membrane which can be undesirable for drug delivery as pores > 100 μm^2 have been shown not to reseal [121] thereby inducing cell death. An intriguing concept of pore formation without the presence of ultrasound contrast agent microbubbles has been hypothesized in recent years, by the concept of spontaneous nano-scale cavitation formation inside the cell membrane bilayer [122–124]. The cavitation threshold and subsequent growth threshold is assumed to be much lower within the bilayer as compared to that in the liquid because of the reduced surface tension and increased solubility of O_2, N_2, and NO in the bilayer. However, detailed experimental and theoretical studies are needed to quantify the existence of such nano-scale pockets in clinically relevant conditions. Moreover, their relation with drug delivery through membrane rupture needs further consolidation.

Moreover, as Pua and Zhong [125] already rightly pointed out in their review in 2009, the multitude of cell models, ultrasound systems, and experimental environments has made clear conclusions about the mechanism of drug uptake difficult. In that respect, since then not much has changed. What also makes it difficult is that most studies only report on drug uptake [121,126–129], or electron microscopy [127,130], or cell electrophysiological measurements [131,132] as outcome, and not the relation between microbubble behavior and drug uptake. On the basis of these studies it is therefore impossible to determine which microbubble behavior stimulates drug delivery. Only a few reports studying the relation between drug delivery and microbubble behavior have been published using optical high-speed imaging [78,95,133–135] or acoustic detection [87,117,131]. An important finding from these studies is that the oscillating microbubbles can deform cells [78,95,134], which could be a trigger for drug uptake. However, more of these studies are desperately needed to elucidate which microbubble behaviors are best suited for drug delivery. Depending on the desired drug uptake route, different microbubble behaviors may be needed. Fig. 8 shows the different drug uptake routes currently known to be induced by insonified microbubbles, namely pore formation (route I, for example [95,126]), stimulated endocytosis (route II, [128]), and opening of cell-cell junctions (route III, [136,137]).

The microbubble behavior needed for route I could be stable cavitation, inertial cavitation, jetting, and microbubbles penetrating cell membranes as these have been shown or are likely to all induce pores. Pore formation occurs at the site where the microbubble acts on the cell [95,138]. Pore sizes as small as 1 nm [139] and as large as >100 μm^2 [121] have been reported. Probably, the degree of pore formation depends on the microbubble behavior with the milder stable cavitation to induce the smallest pores and the more violent inertial cavitation, jetting, and microbubbles traveling through cell membranes to induce the largest pores. Resealing times of pores have been reported to range from milliseconds to several seconds [95,130,135], concluding that the drug uptake via route 1 is transient if the created pore is not too large.

Drug uptake via route II has recently been reported in vitro and in vivo [128,140]. In the study by Meijering et al. [128], endocytosis stimulation was found at the same acoustic parameters that induced pore formation and calcium influx. Other studies not involving microbubbles and ultrasound have shown a direct correlation of endocytosis with intracellular calcium ions $[Ca^{2+}]_i$, reactive oxygen species (ROS), and cytoskeleton changes [141–143]. As both $[Ca^{2+}]_i$ and ROS can be induced by vibrating microbubbles [128,144–148], and cytoskeleton changes have also been reported [145], the mechanistic explanation for route II could be that vibrating bubbles up regulate endocytosis through an increase in $[Ca^{2+}]_i$ and/or (ROS) and/or cytoskeleton changes. The increase in $[Ca^{2+}]_i$ can be explained by influx of Ca^{2+} through pore formation since $[Ca^{2+}]$ outside the cell is much higher [149]. Interestingly, it has also been reported that an induced increase in $[Ca^{2+}]_i$ can spread from one cell into neighboring cells [138,150] following microbubble and ultrasound treatment. From other non-microbubble non-ultrasound studies it is known that an increase in $[Ca^{2+}]_i$ can also be triggered by activation of mechanosensitive ion channels on the cell membrane and/or stimulation of the release of intracellular calcium storage pools [151,152]. Since microstreaming or direct cell deformation caused by oscillating microbubbles are likely to activate mechanosensitive ion channels, the increase of $[Ca^{2+}]_i$ can also be explained without pore formation. In addition, from other non-microbubble non-ultrasound studies, shear stress is known to induce endocytosis [153,154]. Whilst Route I is a short-term route, route II could be a longer term route and therefore could explain why Yudina et al. found drug uptake persisting even 24 hours after microbubble and ultrasound treatment [155].

Evidence for Route III in vivo has been reported by electron microscopy which revealed opening of the endothelial layer in the brain [136] and prostate [137] after ultrasound and microbubble treatment. This route has also been studied in vitro using electrical resistance measurements on cultured endothelial cells [156,157]. In theory, oscillating microbubbles could push apart cells in the endothelial layer, thereby mimicking neutrophils that migrate through the endothelial layer [158,159]. However, more likely is that drug uptake via route III is induced by increased shear stress due to the microstreaming as this is known to induce cell-layer permeability [160,161]. Just as for endocytosis, $[Ca^{2+}]_i$, ROS, and cytoskeleton changes are also reported to be involved in cell-layer permeability [162], which as mentioned at route II can also be induced by vibrating microbubbles.

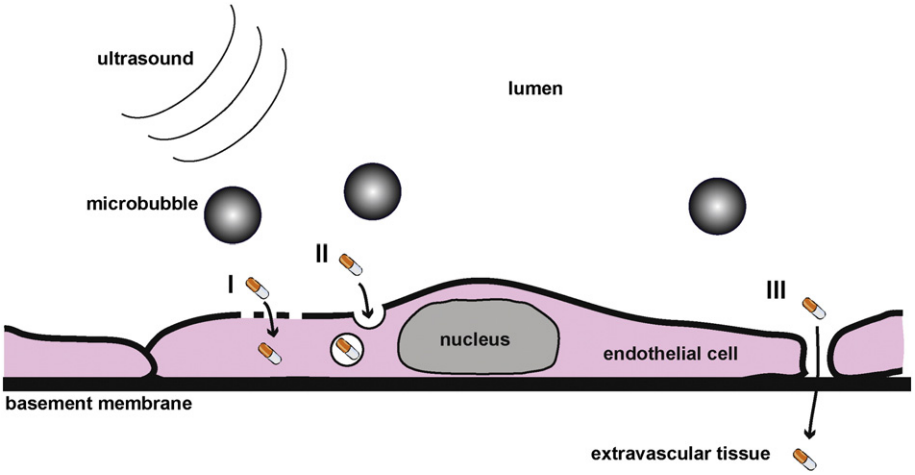

Fig. 8. Concept of microbubble-mediated drug delivery in endothelial cells I) through cell membrane pores, II) via endocytosis, and III) through cell junctions into extravascular tissue. Depending on the site of action of the drug, the appropriate microbubble-mediated drug delivery route could be chosen.

Recently, targeted microbubbles have also shown potential for co-administration [163]. Targeted microbubbles have ligands onto the coating. The ligands can bind to an extracellular membrane protein or receptor that is for example (over)expressed by a diseased cell [164]. Compared to freely circulating microbubbles, targeted microbubbles behave differently in an acoustic field [165–167]. This effect and the difference of bound and free bubbles in drug uptake have not yet been studied well. For example, it is unknown if targeted microbubbles can induce microstreaming or generate jets in the same way as free bubbles. Nevertheless, stable cavitation and inertial cavitation occur and drug uptake has been shown by Kooiman et al. [163]. In addition, this in vitro study showed that vibrating bound CD31-targeted microbubbles induced uptake of the model drug propidium iodide in endothelial cells when the relative vibration amplitude of the microbubbles exceeded the threshold of 0.5 applying a frequency of 1 MHz (6×10 cycles). This uptake was already noticed at acoustic pressure as low as 80 kPa. Propidium iodide was also used as model drug for the targeted microbubble co-administration study by McLaughlan et al. [36]. In this study, the microbubbles were targeted to $\alpha_v\beta_6$ on HCT116 colorectal carcinoma cells. Interestingly, chirp excitations were compared to single frequency excitations with the chirps showing higher sonoporation efficiencies for the polydispersed microbubbles (mean of 2.4 ± 1.3 μm). The highest sonoporation efficiency was demonstrated with the 3–7 MHz chirp and was a factor of 2 higher than for the single frequency excitation at 2.2 or 5 MHz. In line with the resonance behavior discussed in section 2, showing that chirps will excite a larger amount of bubbles at resonance, this study implies that when microbubbles are excited at resonance, sonoporation efficiency is highest. Whether the findings by Kooiman et al. [163] and McLaughlan et al. [36] are only valid for bound microbubbles needs further investigation.

Sonoporation is also influenced by the microbubble-cell type combination as Escoffre et al. [168] showed. They compared sonoporation of five different ultrasound contrast agents using two different cancer cell lines in vitro. There were clear differences in the efficiency between the two cell lines. However, the relevance of using cancer cells to study sonoporation in vitro is questionable as ultrasound contrast agents are blood pool agents [7,16] and therefore only can have contact with endothelial cells and circulating blood cells. Only when cancers invade into the vasculature, which for example has been reported for colorectal cancer [169] and hepatocellular carcinoma (HCC; i.e. primary liver cancer) [170], microbubbles can have contact with cancer cells. Another option is a different route of microbubble administration suggested by Chang et al. [171] in their in vitro study using ovarian cancer cells and targeted microbubbles as drug carrier system. They suggested in vivo intraperitoneal administration as 90% of ovarian cancers are confined to the peritoneum [172]. Consequently, the microbubble behavior inside the peritoneum will be different than in the in vitro or intravascular setting due to confinement as discussed in Section 2.7. Such an alternative route of administration was already successfully used by Delalande et al. as the gene was co-administered with BR14 microbubbles by direct injection in the Achilles tendon in mice [173].

The reason why for in vitro co-administration studies the chosen cell type is mostly a cancer cell could be practical in that they are easy to culture. Therefore the number of studies using endothelial cells remains limited. On the other hand, in vitro studies on endothelial cells are usually done under static conditions, i.e. without flow. Park et al. [174] showed that endothelial cells grown under flow (5 dyne/cm^2; i.e. human venous flow [104]) are less susceptible to sonoporation than when grown under static conditions. More complex in vitro models that more resemble the in vivo situation therefore are justified, and should take into account the cell type that the microbubbles will have contact with.

3.2. Rigid-coated microcapsules

Compared to flexible-coated microbubbles, very few studies investigated the use of rigid-coated microcapsules for co-administration. In 2007 the first study using polymer microcapsules was reported by Mehier-Humbert et al. [175]. In this study, triacylglyceride and polystyrene microcapsules were compared to lipid-coated microbubbles for their ability to transfect GFP plasmid into rat mammary carcinoma cells (MAT B III) in vitro. Interestingly, the rigid-coated microcapsules showed lower transfection rates than the lipid-coated microcapsules but transfection with the microcapsules resulted into higher amount of GFP-copies per transfected cell, suggesting more plasmid copies were delivered per cell with the rigid-coated microcapsules. At the investigated frequency of 1.15 MHz, the triacylglyceride microcapsules showed a clear threshold for transfection. The authors suggested that the microcapsules first have to rupture thereby releasing the gas and creating a free microbubble. This free microbubble is then responsible for the transfection and can vibrate violently, since rupture acoustic pressures are quite high (>300 kPa). This could also explain why the authors have reported a lower peak negative pressure threshold for transfection at 2.5 MHz than at 1.15 MHz, suggesting the triacylglyceride microcapsules were more easily ruptured at 2.5 MHz. When the molecular weight of the polystyrene for the coating of the microcapsules was increased, resulting in a thicker rigid coating, the transfection rate decreased, indicating the thicker coated microcapsules were more difficult to rupture.

The study by Cochran and Wheatley [176] used poly(lactic acid)-shelled microcapsules with a resonance frequencies of 2.5 MHz. Interestingly, at 1 MHz the highest transfection was seen. This suggests that the microcapsules were more easily ruptured at 1 MHz, thus below resonance, thereby releasing the encapsulated gas which induced the transfection. Escoffre et al. [168] investigated the use of polymer microcapsules for co-administration of doxorubicin in vitro in cancer cells with cell death as outcome. In this study the performance of two different polymer microcapsules was compared with lipid-coated microbubbles at 1 MHz and 600 kPa (40 cycles at PRF of 10 kHz for 30 s). Both the polylactide and polylactide-PEG microcapsules were shown to enhance doxorubicin-induced cell death, but the polylactide-PEG microcapsules induced more cell death than the polylactide microcapsules, possibly caused by a lower rupture threshold of the polylactide-PEG microcapsules. When compared to the lipid-coated microbubbles (Vevo Micromarker, BR14, and SonoVue), the polymer microcapsules induced similar therapeutic ratios in U-87 MG human glioblastoma astrocytoma cells. For MDA-MB-231 human breast adenocarcinoma cells, the therapeutic ratio of the rigid-coated microcapsules was similar to BR14, but lower than Vevo Micromarker. This again stresses the importance of choosing the appropriate in vitro model for co-administration studies as well as the type of microbubble.

An optical study on co-administration with polymer microcapsules (S_c, 100% air-filled microcapsules prepared with a shell of pLA-pFO [51]) revealed that cracking of the microcapsule followed by small oscillations of the escaped gas was insufficient to induce sonoporation in human umbilical vein endothelial cells (HUVECs). In this study cells were selected which had only one microcapsule so that the direct relationship between the microcapsule and cell could be studied. The S_c microcapsules showed gas release at 1 MHz, 10 cycles and P_- of 250 kPa followed by a vibration of the free gas bubble with a relative amplitude of 2.7 ± 0.6. However, this did not induce sonoporation of HUVECs as uptake of propidium iodide was not observed in the cells. For a higher P_- of 500 kPa, the relative vibration amplitude of the escaped free microbubble increased to 4.1 ± 0.9 causing PI uptake as shown in Fig. 9a. Selected frames from the high-speed recording of the same microcapsule are shown in Fig. 9b. The high-speed recording revealed that the microcapsule indented at the bottom left corner (frame 29), returned to its original spherical shape (frame 31) after which escape of the encapsulated gas was observed (frame 33). The free gas vibrated violently (see frame 37–46). The escaped bubble existed for less than 80 ms (since it had disappeared in the next experiment 80 ms later). Propidium iodide uptake at 500 kPa was only observed for five out of the nine studied microcapsules. For the four not showing sonoporation, the escaped microbubbles had a low vibration amplitude [163], namely 3.3 ± 0.2 (versus 4.8 ± 0.5). This study indicates that the escaped free gas microbubble is indeed responsible for the sonoporation, and not the polymer microcapsule itself. Interestingly, the observed relative vibration amplitude is ~8 times higher than what we reported for targeted lipid-coated microbubbles [163]. This suggests that lipid-encapsulated gas microbubbles may have a lower threshold for sonoporation than polymer microcapsules/non-coated microbubbles. On the other hand, no marked differences were observed between pLA–pFO polymer microcapsules and lipid-coated microbubbles in the in vivo study by Böhmer et al. [177]. In this co-administration study, the albumin-binding dye Evans Blue was used as model drug in mice. A very long burst was applied as well as very high pressures (1.2 MHz at 2 MPa and 10,000 cycles using the Therapy and Imaging Probe System from Philips), which were well above the threshold for sonoporation for both bubble types. For the polymer microcapsules, the effect of cycle length and time of administration of Evans Blue were also evaluated in muscle. Pulses of 100 cycles resulted in a significantly smaller area of Evans Blue uptake in muscle when compared to pulses of 10,000 cycles, which the authors contributed to an augmented

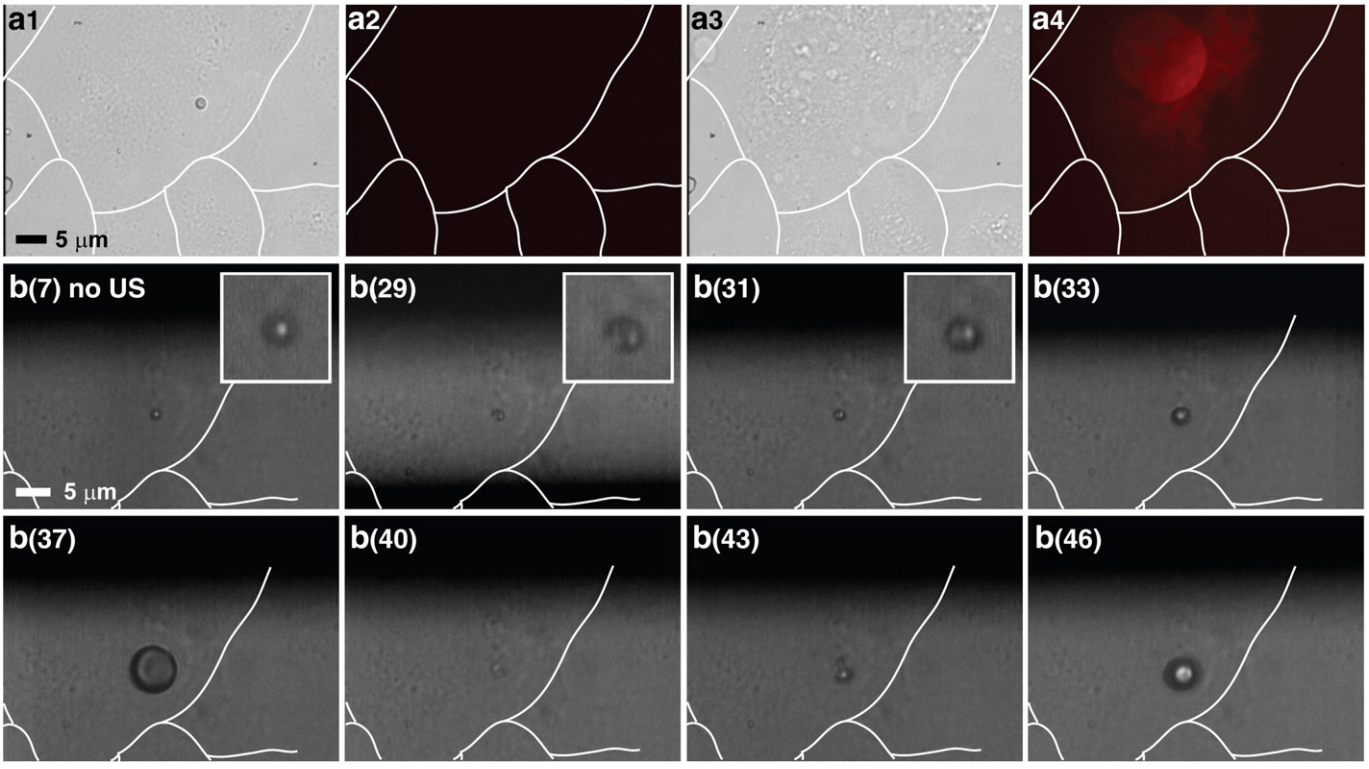

Fig. 9. a) Induction of PI uptake in HUVEC cells (PN 10) by insonified S_c microcapsule. a1 + a2) Before insonification; a3 + 4) Three minutes after insonification at 500 kPa peak negative pressure with a 1 MHz transducer, 10 cycles (a1 + a3 bright field; a2 + a4 fluorescence). PI uptake (25 μg/ml) was detected using fluorescence (excitation 510–550 nm, emission 590 nm) on a BX2 Olympus microscope (60× objective) and recorded with a high sensitivity CCD camera (LCL-902 K, Watec, Orangeburg, NY, USA). b) Eight selected frames out of Brandaris-128 high-speed camera recording (12 million frames per second) of same microcapsule as in a. Frame number of recording is given in top left corner in between brackets; insets (5 × 5 μm) in frame number 7, 29, and 31: zoomed in on microcapsule. Endothelial cell borders (determined from calcein AM staining) are indicated by white lines.

diffusion due to the higher amount of cycles. Interestingly, administration of the dye directly after ultrasound and microcapsule treatment resulted in an even higher amount of uptake than when it was given simultaneously with the microcapsules. Even when the dye was administered 60 min after ultrasound and microcapsule treatment, there was still enhanced uptake, even though this was lower and at a smaller area than when given before or directly after treatment. This indicates that prolonged effects can also be induced with microcapsules, not just with lipid-coated microbubbles.

Cell viability has been studied in in vitro studies. Mehier-Humbert et al. [175] reported cell viabilities above 75% for triacylglyceride and polystyrene microcapsules. Cochran and Wheatly [176] reported cell viabilities between ~60–95% for the poly(lactic acid) microcapsules. The cell viability was dependent on the ultrasound setting and was inversely related to the transfection efficiency: the higher the transfection, the lower the cell viability. This phenomenon has also been reported for studies using lipid-coated microbubbles [178], and indicates there is a fine balance between optimal drug uptake and inducing irreversible cell damage. Therefore, the more violent the microbubble behavior, the better does not hold if it is important not to compromise cell viability.

In conclusion, rigid-coated microcapsules can induce drug uptake. From the very few studies directly comparing rigid-coated microcapsules to flexible-coated microbubbles, it can be concluded that the efficacy is similar. The longevity of an uncoated microbubble is however shorter than a coated microbubble and therefore the flexible-coated microbubbles are expected to have a longer interaction time with cells than escaped uncoated microbubbles from ruptured microcapsules. It is therefore questionable whether rigid-coated microcapsules can induce microstreaming. It is however likely that an increase in $[Ca^{2+}]_i$ occurs as bio-effect because of pore formation (i.e. route I), which could form the basis for stimulating drug uptake via route II and III as described in section 3.1. However, this needs further investigation.

4. Drug carrier system

4.1. Flexible drug-loaded microbubbles

Flexible-coated microbubbles can be used as drug carrier system by either linking drugs to the coating of the microbubble, adsorbing drugs to the coating, incorporating the drugs within the coating or adding an additional drug reservoir into the core of the microbubbles, see Fig. 10. Examples of drug carrier systems and the ultrasound settings used to trigger the release of the drug from the microbubbles are given in Table 1. Acoustic parameters ranged from 20 kHz to 12 MHz in frequency and from 13 kPa to 7 MPa in peak negative pressure. For the majority of these drug-carrying microbubbles, an in-depth investigation as to which ultrasound parameters are optimal to induce drug release are simply lacking. In the majority of these studies, only one single ultrasound frequency and one single acoustic pressure are studied (see Table 1). Some studies do map out more the acoustic parameter space. One example is the in vitro study by Phillips et al. [179] who incorporated the drug rapamycin, an antiproliferative drug, into the coating of lipid-coated microbubbles. They varied the peak negative pressure and pulse length, keeping the ultrasound frequency and duty cycle fixed at 1 MHz and 0.5%, respectively. In addition, they took into consideration the type of cell (smooth muscle cells) that the microbubble and drug would need to act upon in vivo. Phillips et al. found that an increasing peak negative pressure or pulse length decreased the proliferation of smooth muscle cells. For at least 50% reduction in proliferation, a peak negative pressure of 400 kPa and a pulse length of more than 10 cycles was required, which suggests the occurrence of bubble destruction, followed by the release of the drugs. In another study by Phillips et al. [180], plasmid DNA-loaded microbubbles were investigated to transfect smooth muscle cells in vitro and in vivo. From the tested acoustic parameters at a frequency of 1 MHz, 50 cycle pulses at a PRF of 100 Hz, 300 kPa peak negative pressure gave maximal gene transfection in vitro. Lower or higher peak negative pressures resulted into lower gene transfection, which is contradicting with the common observation that transfection and cell death increase with increasing pressures. However, the authors provide no explanation for this remarkable result. Interestingly, 1 MHz frequency 600 kPa pressure ultrasound gave similar in vitro transfection as with a clinical linear array 5 MHz transducer (~1.6 MPa), suggesting there could be more than one optimal acoustic parameter. Chen et al. [181], who incorporated adenovirus encoding the luciferase gene (AdCMV-luc) into lipid-coated microbubbles, also studied multiple ultrasound parameters in vivo. Triggered ultrasound induced more luciferase activity in the rat heart than continuous wave ultrasound. This can be attributed to refilling of the capillary bed with microbubbles in between ultrasound triggers, which results in an increased number of microbubbles within the treatment area when compared to continuous wave ultrasound. Luciferase activity was lowest when the microbubbles were insonified at 12 MHz and highest at 1.3 MHz, despite a constant MI of 1.6, suggesting the microbubbles were more effective at releasing their payload at the lower frequency. No significant difference was found between ultraharmonic (single pulse per scan line) and Power Doppler imaging (multiple pulses per scan line) modes. For a frequency of 1.3 MHz, at the peak negative pressure of 1.8 MPa, luciferase activity was higher than at the peak negative pressure of 1.4 MPa, suggesting that at the peak negative pressure of 1.4 MPa maximum drug release was not yet achieved. At a higher peak negative pressure of 2.3 MPa, luciferase activity was similar for plasmid luciferase DNA incorporated in the coating as for the adenovirus gene incorporated in the coating at the lower peak negative pressure of 1.8 MPa, suggesting that acoustic parameters need to be optimized for each drug. In this study, the luciferase expression was consistently found higher in the anterior wall than in the posterior wall of the heart, which the authors contributed to attenuation in the left ventricle cavity.

The addition of an additional drug reservoir such as oil drastically changes the acoustic behavior of the microbubbles as it changes the coating properties and thickness of the coating, as shown by May et al. [82]. The oil layer thickness within the lipid-coated microbubbles (by the authors referred to as acoustically active lipospheres (AALs)) was 0.3–1.5 μm, and was used to incorporate hydrophobic drugs such as paclitaxel [182,183]. Acoustical studies using ultrasound frequencies from 1.5 to 2.5 MHz and pressures from 1.6 to 3.4 MPa (5-cycle pulses) revealed that the AALs were acoustically active [82]. Whilst expansions and fragmentation was observed for triacetin-oil filled AALs, soybean-oil filled AALs were significantly more difficult to fragment and no

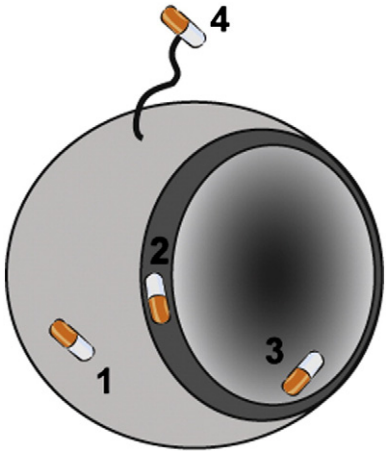

Fig. 10. Schematic overview of ways to incorporate drugs into microbubbles/microcapsules (not drawn to scale). Drugs can be adsorbed to the coating (1); incorporated in the coating (2); incorporated in the core (3), or attached to the surface (4) of the microbubble.

Table 1
Examples of flexible coated microbubbles as drug carrier system and the acoustic parameters used to trigger drug release.

Incorporation drug	Coating material	US frequency	Pressure/intensity	Cycles/PRF	Incorporated drug	In vitroo	In vivo	Ref
Linked to coating	Lipid	1.5 MHz	1.1 MPa	5-cycle pulse (+1.3-s radiation force pulse at 3 MHz and 150 kPa)	Latex bead	x		[193]
	Lipid	1 MHz	2 W/cm^2	10% duty cycle for 10 s	Lipoplexes (complexes of DNA with PEGylated liposomes)	x		[194]
	Lipid	1 MHz	2 W/cm^2 (170 kPa)	50% duty cycle, moving in 15 s over whole Opticell	Doxorubicin in liposomes	x		[195]
	Lipid	1 MHz	2 W/cm^2	20% duty cycle, moving in 15 s over whole Opticell	Doxorubicin in liposomes	x		[196]
	Lipid	1.5 MHz	1.2 MPa	Intermitted with 0.1 MPa	MicroRNA in liposomes		x	[197]
	Lipid	1 MHz	7 MPa	5 pulses with 100,000 cycle length at 1 Hz	Calcein or thrombin in liposomes	x		[198]
Adsorbed to coating	Lipid	1 MHz 2.5 MHz	800 kPa 500 kPa	5-cycle pulse	DNA	x		[199]
	Lipid	1.75 MHz	1.1 MPa 1.04/1.14 MPa	30 Hz, 10 s N.D.	Plasmid DNA	x	x *	[200]
	Lipid	1 MHz 5 MHz 1 MHz 5 MHz	0–950 kPa 1.6 MPa 0.6 MPa 1.6 MPa	0–100 cycles, 0.5% duty cycle, ~5 s per cell 5 cycles, PRF 5 kHz equivalent duty cycle 5 cycles, PRF 5 kHz for 1 min	Plasmid DNA	x	 x	[180]
	Lipid	1.3 MHz	1.7–1.9 MPa	Every 4–6 cardiac cycles in end systole	Plasmid DNA		x	[201]
	Lipid	1.3 MHz	1.8 MPa	Bursted for 30 min	Plasmid DNA		x	[202]
	Lipid	1.0 MHz 1.5 MHz	200–300 kPa* 200 kPa	PRF 100 Hz, ~5 s per cell PRF 8 kHz, ~5 s per cell	Plasmid DNA (+targeting)	x		[191]
	Lipid	1 MHz	5 W/cm^2	25% duty cycle for 5 min	Plasmid DNA (+targeting)		x	[189]
	Lipid	1.6 MHz	0.6, 1.0, 1.8 MPa	PD, pulsing interval 5 s, PRF 2.5 kHz for 10 min	Plasmid DNA (+targeting)		x	[190]
	Albumin	20 kHz 2 MHz	46 kPa 13 kPa	CW for 3 min	Antisense oligonucleotide		x	[203]
	Albumin	N.D.	2.5 W/cm^2	8 times 1 min 2 min	plasmid DNA	x	 x	[204]
	Albumin	1.3 MHz	1.7 MPa	burst of 3 frames very 4–6 cardiac cycles	adenovirus gene		x	[205]
	Albumin + polymer	1 MHz	1 W/cm^2	50% duty cycle for 30 s	Plasmid DNA	x		[206]
Within coating	Lipid	1 MHz	4 W/cm^2 (131 kPa) 1 W/cm^2	50% duty cycle for 30 s 50% duty cycle for 20 s	Doxorubicin	x		[207]
	Lipid	300 kHz	2 W/cm^2	CW 10 s on, 10 s off for 6 min	Docetaxel		x	[208]
	Lipid	1 MHz	0.5 W/cm^2	CW 10 s on, 5 s off for 2 min	Paclitaxel		x	[209]
	Lipid	1 MHz	2 W/cm^2	CW 10 s on, 10 s off for 6 min	10-Hydroxycamptothecin		x	[210]
	Lipid	1 MHz	0.3–1.1 MPa 0.3–0.6 MPa	PRF 1, 2, 5 and 10 Hz, 1000, 5000, and 10,000 cycles PRF 1, 2, 5, and 10 Hz (1, 2 and 4 sites, 1 min per site)	BCNU	x	 x	[211]
	Lipid	1 MHz	0.5 MPa 0.7 MPa	10,000 cycles, PRF 5 Hz for 1 min at 2 sites 10 ms burst, 5% duty cycle, PRF 5 Hz, 1 min at 2 sites	BCNU (+ targeting)	x	 x	[192]
	Lipid	1 MHz	200–800 kPa	0.5% duty cycle; 1, 10, or 15 cycles for 6 min (8.3 s per cell)	Rapamycin	x		[179]
	Lipid	5 MHz	1.5 MPa	5 cycle pulse every 200 microseconds (3 s on, 2 s off), 8 min (+ 1.2 MHz radiation force at 135 kPa)	rapamycin		x	[212]
	Lipid	1.3 MHz	1.8 MPa	CW for 2 min 4–6 bursts with 1.5–2.5 s between bursts for 30 min	siRNA	x	 x	[213]
	Lipid	1.3 MHz	1.4–2.3 MPa 1.8 MPa 1.8 MPa 5 MHz 12 MHz	1 (UH): Burst of 4 frames gated to every 4th heartbeat at end-systole 2 (UH): CW 1 (PD) 1 (UH) 1 (UH)	Adenovirus gene/plasmid DNA		x	[181]
	Lipid	300 kHz	2 W/cm^2	CW for 5 s separated by 5 s for total of 6 min	Plasmid DNA + peptide		x	[214]
	Lipid Albumin	1.3 MHz	1.7 MPa	4 frames every 4 cardiac cycles	Plasmid DNA	x		[215]
	Albumin	1 MHz	1, 2, 3, 4 W/cm^2	30 s	Luciferin		x	[216]
Drug reservoir in bubble	Lipid with oil layer	2.5 MHz, 2.5 MHz + 100 kHz CW, 2.5 MHz + 100 kHz PW	2.5 MHz: 100 kPa, 100 kHz: 0.8 W/cm^2	2.5 MHz: PRF 1 kHz, 100 kHz PW: 7% duty cycle	Paclitaxel	x		[182]
	Lipid with oil layer	2 MHz 1 MHz	0.95 MPa 2 MPa	6 5-cycle pulse 3 5-cycle pulse	Paclitaxel	x	 x	[183]

UH = ultraharmonic imaging; CW = continuous wave; PW = pulsed wave; PD = Power Doppler imaging; N.D. = not defined; PRF = pulse repetition frequency; BCNU = 1,3-bis(2-chloroethyl)-1-nitrosourea; * determined as optimal acoustic parameters from previous study [180].

bubble expansions were observed during insonification. This can be explained by the higher viscosity of soybean oil compared to triacetin-oil, resulting in an increased damping. Expansion and fragmentation were more pronounced at a frequency of 1.5 MHz than at 2.5 MHz, even more so for AALs smaller than 3 μm, indicating the AALs were closer to resonance at 1.5 MHz. Compared to lipid-coated microbubbles without oil, the expansion behavior of AALs was similar for the first cycle, but whilst lipid-coated microbubbles fragmented at the first cycle, fragmentation of the AALs occurred only at the fifth or higher number of cycles. Fragmentation was also studied and was shown to depend upon the initial radius of the AALs. AALs smaller than resonance size underwent symmetric collapse and produced a set of small, equally-sized fragments. Pinch-off was observed for AALs larger than twice the resonance radius, with one fragment containing a large fraction of the original volume. This finding is consistent with the period-doubling and splitting behavior shown in Fig. 3. Release as well as therapeutic efficacy was demonstrated both in vitro and in vivo [182–184]. The addition of radiation force to the therapeutic ultrasound and/or targeting the AALs to the biomarker $\alpha_v\beta_3$ resulted in a more pronounced release of the encapsulated (model) drug as the AALs were pushed towards as well as adhering to the neighboring wall thereby releasing their payload closer to the cells [184].

Incorporating drugs into another drug carrier system such as a liposome and linking this liposome to the coating of microbubbles has also been studied by several groups (for examples see Table 1). Whilst Kheirolomoom et al. [185] reported no difference in microbubble behavior between their microbubble-liposome complexes and previously reported microbubble behavior (2.25 MHz and 200 kPa peak negative pressure, 3-cycle pulse), Luan et al. [186] did report differences in acoustic behavior between microbubbles with and without liposomes attached. Although the shell elasticity was similar, the shell viscosity was significantly higher for liposome-loaded microbubbles. Also, the liposome-loaded microbubbles had a higher pressure threshold for the onset of microbubble vibrations, indicating that the attachment of the liposomes contributed to a change of the microbubble behavior. At the moment, the mechanisms of drug release from the microbubble-linked liposomes is being studied [99,187,188], resulting in recordings such as shown in Fig. 7 for fluorescent liposome recordings, which will aid in understanding and optimizing drug release for this high-capacity drug-loading system.

Although targeted flexible-coated microbubbles have been reported as drug carrier system ([171,189–191], see Table 1), the mechanism or added value of the targeting capacity of these microbubbles is in its infancy. Chang et al. [171] showed that their targeted microbubbles were more efficient in transfecting cells in vitro as compared to their non-targeted microbubbles. However, this difference could also have resulted from the difference in microbubble size. The targeted microbubbles had a 0.9 μm larger mean than the non-targeted microbubbles. As the applied ultrasound of 1 MHz was unchanged for both types of microbubbles, the non-targeted microbubbles were therefore further off resonance than the targeted microbubbles which leads to smaller oscillation amplitudes for the non-targeted microbubbles (see section 2). Both Phillips et al. [191] and Xie et al. [190] respectively found a 5.5 times higher (in vitro) and 5 times higher (in vivo) transfection efficiency for their targeted plasmid DNA loaded microbubbles compared to their plasmid DNA loaded non-targeted microbubbles. Fan et al. [192] also showed a higher drug release in vitro and in vivo for targeted than non-targeted BNCU-drug loaded microbubbles. Hence, these recent studies clearly show that targeting of drug-loaded microbubbles is more effective. Whether this effect can be attributed to differences in microbubble dynamics or the fact that the release of the drug occurs closer to the cell, remains to be investigated.

4.2. Rigid drug-loaded microcapsules

Several groups have reported on the fabrication of rigid-coated microcapsules as (model) drug carrier system. Drugs can either be linked [217] or adsorbed [218–220] to the coating, or encapsulated in the coating itself [218–224] or within a drug reservoir within the core of the microcapsule [51], see Fig. 10. Not all groups that developed drug-loaded rigid-coated microcapsules investigated in depth whether the drug loading affected the microcapsule behavior or how the drug was released from the microcapsules upon insonification. However, this is important as ultrasound needs to effectively trigger the release of the drug from the microcapsule. Therefore, the response of the microcapsule to ultrasound is important.

Even though the coating of microcapsules is rigid, linkage of drugs to the coating can induce alterations of the rigid coating and thereby alter the acoustic behavior of the microcapsules as reported by Wheatley et al. [217]. They linked tumor necrosis factor-related apoptosis-inducting ligand (TRAIL) to their poly lactide-coated microcapsules, and observed a reduction in ultrasound backscatter and ultrasound stability at 5 MHz frequency ultrasound. This was attributed to the ligation of TRAIL to the poly lactide coating which takes place under aqueous conditions, initiating polymer hydrolysis, which resulted in a destabilization of the coating. In addition, the chemical modifications needed for the ligation could also have changed the structure of the coating. Eisenbrey et al. [219] also reported a reduction of ultrasound enhancement when doxorubicin was surface absorbed to the poly lactide coating of these poly lactide-coated microcapsules after fabrication. No changes in ultrasound enhancement were observed when doxorubicin was surface absorbed during fabrication or incorporated in the coating, suggesting the cause was hydrolytic damage to the coating during the doxorubicin adsorption to the coating, as well as a second freeze drying step. Nonetheless, the TRAIL-microcapsules and doxorubicin-microcapsules were acoustically active. The 5 MHz insonification frequency used in these studies was chosen based on previous studies in which the microcapsules were shown to resonate between 3 and 5 MHz [225]. Another anti-cancer drug, paclitaxel, was also loaded into the poly lactide-coated microcapsules by the same group [221]. These microcapsules showed less acoustic in vitro stability compared to non-drug loaded microcapsules, indicating that the inclusion of the hydrophobic drug paclitaxel also influences the acoustic behavior of the microcapsules. Acoustically less stable microcapsules were also observed in vitro for microcapsules with doxorubicin incorporated in the coating [219] which could be favorable drug release, but this was not investigated. For the paclitaxel-loaded microcapsules [221], the increased mean size of the microcapsules with increasing initial loading amounts of paclitaxel could have attributed to this as a larger microcapsule is likely to have a different resonance frequency. Differences in mean size were not observed for the doxorubicin-loaded microcapsules [219]. However, the size and/or acoustic behavioral changes for these microcapsules were likely not detrimental in terms of drug release as in vitro cell death was successfully demonstrated for the ultrasound-treated paclitaxel-loaded microcapsules.

How the drug is incorporated into the microcapsule also plays a role for its ultrasound-triggered release as reported by Eisenbrey et al. [218]. For shell-incorporated doxorubicin loaded microcapsules, an increase in in vitro cell death was observed when the applied peak negative pressure was increased, suggesting a more pronounced release from a ruptured coating. In contrast, for surface absorbed doxorubicin, no significant increase in cell death was observed when ultrasound was applied, suggesting that doxorubicin was already released even without ultrasound as trigger. Conversely, free doxorubicin in combination with the microcapsules and ultrasound (i.e. co-administration) showed a significantly higher cell death when compared to shell-incorporated doxorubicin. This suggests an impartial release of the doxorubicin from the doxorubicin-loaded microcapsules (5 MHz, 100 PRF, 0.94 MPa).

Drug release and efficacy was studied in more detail by the group of Wheatley. They reported that ultrasound ruptured the microcapsules into 200–400 nm fragments [217,226]. The extravasation of the fragments into the tumor interstitium could be facilitated by the enhanced permeation and retention (EPR)-effect [227]. In addition, extravasated

shell fragments biodegrade slowly, giving a sustained local drug release, possibly for days to weeks [228]. Translation of the in vitro settings to the in vivo situation is difficult as in vitro 5 min of insonification was needed which is not feasible in vivo as the microcapsules circulate. On the other hand, the observed increased doxorubicin level in the peripheral liver tumor in rabbits after ultrasound treatment suggests that doxorubicin is also released from the microcapsules in vivo [226]. This was further demonstrated in rats bearing hepatomas where the increased doxorubicin level was observed in the tumor even 14 days after treatment [229]. Also, higher doxorubicin levels in the tumor and tumor growth arrest were observed following ultrasound and doxorubicin-loaded microcapsule treatment when compared to freely administered doxorubicin, thus showing the efficacy of the drug-loaded microcapsule approach compared to the traditional systemic administration.

The inclusion of a drug carrier reservoir such as oil into the microcapsule will influence the acoustic behavior of the microcapsule as this will replace part of the gas core [51]. For pLA-pFO microcapsules, the resonance frequency decreased with the inclusion of the oil. This is contradictive to the general rule that smaller gas bubbles will have higher resonance frequencies [40]. However, the oil increased the coating to gas ratio which likely increased damping of the encapsulated gas bubble, which could result in a lower resonance frequency [17]. In addition, the threshold for acoustic events at a frequency of 1 MHz was higher, which is in agreement with the assumption of increased damping. A pilot in vivo study was reported on the therapeutic effect of this drug carrier system [230]. It showed that tumor growth was suppressed after treatment with paclitaxel-loaded half-oil filled microcapsules and ultrasound.

5. Conclusion and future perspectives

Ultrasound stimulated drug delivery with microbubbles has now been around for more than two decades. Since then, researchers are trying to unravel the microbubble behavior that stimulates and controls drug uptake. Despite the advances in the field, like high frame rate and fluorescence imaging, modeling, cell responses and animal studies, there are still many gaps in understanding the full mechanism. This is shown in Fig. 11, in which we present a schematic overview of the entire cascade from bubble vibration up to animal and human clinical therapeutic effects. The bubble vibration is dictated by the acoustic ultrasound parameters, like frequency, pulse length, amplitude and repetition rate, and causes hydrodynamic effects around the oscillating microbubbles, as described in section 2. The right hand side depicts the possible cellular response, as described in sections 3 and 4. We dubbed the link between the hydrodynamics and the cellular response as the mechanical link. We identified throughout this review that this link is a largely unexplored area, i.e., there is a large knowledge gap for the response of cells to mechanical stimulation on time scales ranging from nanoseconds to milliseconds and even seconds. In virtually all delivery studies referred to in this review, the two areas, the microbubble behavior and the cellular response, are addressed simultaneously. This has turned out to be too complicated. Only the begin and end points have been studied resulting in speculative interpretations for the path in between. We believe that this simultaneous approach introduces too many unknowns, slowing down the convergence of results towards effective drug delivery. One of the reasons why the mechanical link has been studied so rarely may be due to the large range in time scales. The time scale of the microbubble vibration is nanosecond to microsecond, which is many orders of magnitude smaller than the time scale of physiological effects (milliseconds), let alone that of biological effects (seconds to minutes) and clinical relevance (days to months). This requires the combination of different imaging systems, from nanoseconds to minutes that look at the same region of interest. Moreover, cell death and drug delivery can only be monitored indirectly, typically by fluorescent staining, requiring specialized equipment. Last but not least, any model should match the final application as good as possible, including a correct cell type, temperature, stiffness, dimension, fluid, etc. In the light of the above considerations it is not a surprise that the exact mechanism of ultrasound stimulated drug delivery with microbubbles is still in its infancy even after two decades, and that current efforts are still going on.

To unravel the complete chain as shown in Fig. 11, we propose first to disconnect microbubble behavior and cellular response. Microbubble behavior has been widely studied in the past decades, and only few unknowns remain. On the contrary, cellular response to mechanical stimulation on nanoseconds to milliseconds time scale is largely unexplored. We imagine experiments in which the stimulation is provided by mechanical actuators with micron-sized tips, and microfluidic channels in which fluid can provide streaming on very small time and spatial scales. We are confident that with such bubble-independent experiments the cellular response to mechanical stimulation can be elucidated much more clearly. Then, microbubbles can be re-introduced, to investigate whether different ultrasound parameters favor one over the other drug delivery route or whether all occur at the same time.

Once the mechanisms have been clarified more, the combination can be followed up again. One possible path is the combination of high-speed and fluorescence cameras, to measure the complex

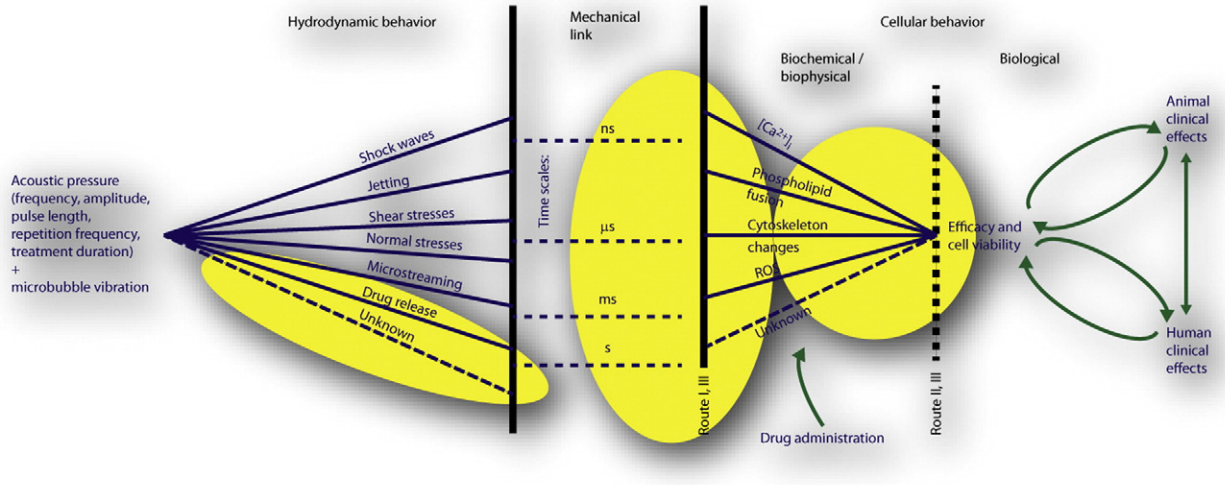

Fig. 11. Schematic picture of the relation between hydrodynamical behavior, cellular behavior, and ultimate clinical effects. Knowledge gaps are emphasized with yellow ellipses.

microbubble-cell behavior and interaction directly. We strongly believe that the latest developments in these directions will reveal more clearly the relation between microbubble behavior and drug delivery. These considerations also massively favor the development of in vivo or ex vivo animal models, such as chicken embryos, various rat organs or even micro-organisms, in which direct intravital microscopy has been shown feasible.

All in all, various general settings have been identified over the past years. Firstly, a frequency around 1 MHz causes the highest transfection, clearly higher than 3 or 5 MHz. Secondly, microbubbles should be excited at or around their resonance frequency to reach the highest oscillation amplitude, resulting in the potential optimal interaction with its surroundings. Most likely this resonance issue is related to the first point since the in vitro resonance frequency of the microbubbles is in general between 1 and 2 MHz. Thirdly, in vivo studies have shown that a shorter burst (<1 ms) has higher efficacy than a long burst (order > 100 ms), most likely because after the 100 ms, all bubbles have disappeared. And fourthly, that intermittent insonification gives better results than continuous insonification since it allows replenishment of the entire region of interest.

With respect to the optimal pressure regime, no consensus exists. The pressure regimes reported for successful in vitro or in vivo drug delivery varies from 80 kPa up to 1.9 MPa. In these regimes both stable cavitation (characterized by mild oscillations) and inertial cavitation (characterized by violent effects such as jets and collapses) will occur. For the low acoustic pressures (<200 kPa) predictive models of in vitro microbubble behavior can be derived from present theory and experiments, but the applicability for the in vivo situation, with blood, cells, and flow, is largely unknown. Yet, few experimental studies at least show that non-spherical oscillations, jetting, and collapse can occur in an in vivo situation at pressure levels relevant for drug delivery. Yet, the control over the microbubble behavior for drug delivery is essential as it is also known that vibrating microbubbles can induce cell death, and even hemorrhage in vivo [231,232] which could be an unwanted side-effect.

With respect to the drug delivery method, co-administration and drug-loaded microbubble or microcapsules, we have not found any study that compares these methods directly in vivo. On the contrary, it would be logical to assume that drug-loaded microcapsules will decrease systemic concentrations of drugs. Yet, to this moment it is not known which approach will give the best overall result. Caution should be given to various current experimental models and setups. First, we noticed that many studies use cancer type cells as model in drug delivery. Yet, microbubbles are injected intravenously, and drugs delivered through or by microbubbles will first have to cross the endothelial barrier to reach the cancer cells. This barrier should be taken into account when conclusions on in vivo application can be derived from the experiments. Second, many researchers make use of a monolayer of cells attached to a rigid membrane (such as an OptiCell). The microbubble oscillation will be affected by the rigid membrane despite the intermediary cell monolayer, leading to, for example, jets directed towards the stiff wall. On the contrary, tissue generally has much lower elasticity, and the bubble behavior will be significantly different. In such a system it could be possible that jets will be directed *away* from the vessel wall instead of towards. It is recommended to develop models with a soft wall, similar to that of a vessel. These points show that, to have real clinical relevance, models and setups should be chosen with care.

Acknowledgments

This research is partly supported by the Center for Translational Molecular Medicine and the Dutch Heart Foundation (PARISk), and by NanoNextNL, a micro and nanotechnology consortium of the Government of the Netherlands and 130 partners. This work is also partly financed by the Foundation for Fundamental Research on Matter FOM and the Technology Foundation STW. It is also supported by TAMIRUT, a Specific Targeted Research (STReP) project supported by the 6th Framework Programme of the European Commission in the Nanosciences, Nanotechnologies, Materials and new Production Technologies area under contract number NMP4-CT-2005-016382, by the Innovation Subsidies collaborative projects by the Dutch Ministry of Economic Affairs under nr. IS042035, and by the Sonodrugs Project (NMP-2008-213706). It is also supported by the Interuniversity Cardiology Institute of the Netherlands (ICIN), and through a personal 2012 ICIN Fellowship (KK). The authors thank Dr. Marcel R. Böhmer and Ceciel Chlon from Philips Research Europe, Eindhoven, for providing the pLA–pFO microcapsules.

References

[1] R. Gramiak, P.M. Shah, Echocardiography of the aortic root, Invest. Radiol. 3 (1968) 356–366.
[2] B.B. Goldberg, J.-B. Liu, F. Forsberg, Ultrasound contrast agents: a review, Ultrasound Med. Biol. 20 (1994) 319–333.
[3] D. Cosgrove, Ultrasound contrast agents: an overview, Eur. J. Radiol. 60 (2006) 324–330.
[4] M. Postema, O.H. Gilja, Contrast-enhanced and targeted ultrasound, World J. Gastroenterol. 17 (2011) 28.
[5] S. Kaul, Myocardial contrast echocardiography: a 25-year retrospective, Circulation 118 (2008) 291–308.
[6] A.L. Klibanov, Ultrasound contrast agents: development of the field and current status, Top. Curr. Chem. 222 (2002) 73–105.
[7] C. Greis, Ultrasound contrast agents as markers of vascularity and microcirculation, Clin. Hemorheol. Microcirc. 43 (2009) 1–9.
[8] T. Faez, M. Emmer, K. Kooiman, M. Versluis, A.F. van der Steen, N. de Jong, 20 years of ultrasound contrast agent modeling, IEEE Trans. Ultrason. Ferroelectr. Freq. Control 60 (2013) 7–20.
[9] J. Wu, W.L. Nyborg, Ultrasound, cavitation bubbles and their interaction with cells, Adv. Drug Deliv. Rev. 60 (2008) 1103–1116.
[10] S. Hernot, A.L. Klibanov, Microbubbles in ultrasound-triggered drug and gene delivery, Adv. Drug Deliv. Rev. 60 (2008) 1153–1166.
[11] A.L. Klibanov, Microbubble contrast agents: targeted ultrasound imaging and ultrasound-assisted drug-delivery applications, Invest. Radiol. 41 (2006) 354–362.
[12] K.W. Ferrara, Driving delivery vehicles with ultrasound, Adv. Drug Deliv. Rev. 60 (2008) 1097–1102.
[13] P.A. Dijkmans, L.J. Juffermans, R.J. Musters, A. van Wamel, F.J. ten Cate, W. van Gilst, C.A. Visser, N. de Jong, O. Kamp, Microbubbles and ultrasound: from diagnosis to therapy, Eur. J. Echocardiogr. 5 (2004) 245–256.
[14] K.W. Ferrara, M.A. Borden, H. Zhang, Lipid-shelled vehicles: engineering for ultrasound molecular imaging and drug delivery, Acc. Chem. Res. 42 (2009) 881–892.
[15] ICUS, What is CEUS?, in: http://www.icus-society.org/about-ceus/ .
[16] J.M. Correas, O. Helenon, L. Pourcelot, J.F. Moreau, Ultrasound contrast agents. Examples of blood pool agents, Acta Radiol. Suppl. 412 (1997) 101–112.
[17] T.G. Leighton, The Acoustic Bubble, Academic Press, London, 1994.
[18] H. Medwin, Counting Bubbles acoustically: a review, Ultrasonics (1977) 7–13.
[19] C.K. Holland, C.X. Deng, R.E. Apfel, J.L. Alderman, L.A. Fernandez, K.J. Taylor, Direct evidence of cavitation *in vivo* from diagnostic ultrasound, Ultrasound Med. Biol. 22 (1996) 917–925.
[20] F. Vignon, W.T. Shi, J.E. Powers, E.C. Everbach, J. Liu, S. Gao, F. Xie, T.R. Porter, Microbubble cavitation imaging, IEEE Trans. Ultrason. Ferroelectr. Freq. Control 60 (2013) 661–670.
[21] N. Kamiyama, F. Moriyasu, Y. Mine, Y. Goto, Analysis of flash echo from contrast agent for designing optimal ultrasound diagnostic systems, Ultrasound Med. Biol. 25 (1999) 411–420.
[22] L. Rayleigh, VIII. On the pressure developed in a liquid during the collapse of a spherical cavity, The London, Edinburgh, and Dublin Philosophical, Mag. J. Sci. 34 (1917) 94–98.
[23] M. Plesset, The dynamics of cavitation bubbles, J. Appl. Mech. 16 (1949) 227–282.
[24] B.E. Noltingk, E.A. Neppiras, Cavitation produced by ultrasonics, Proc. Phys. Soc. Sec. B 63 (1950) 674–685.
[25] E. Neppiras, B. Noltingk, Cavitation produced by ultrasonics: theoretical conditions for the onset of cavitation, Proc. Phys. Soc. Sec. B 64 (1951) 1032–1038.
[26] H. Poritsky, The collapse or growth of a spherical bubble or cavity in a viscous fluid, Proc. First Nat. Cong. Appl. Math. (1952) 813–821.
[27] C.E. Brennen, Cavitation and Bubble Dynamics, Oxford University Press, 1995.
[28] S. Hilgenfeldt, D. Lohse, M. Zomack, Response of bubbles to diagnostic ultrasound: a unifying theoretical approach, Eur. Phys. J. B 4 (1998) 247–255.
[29] N. de Jong, A. Bouakaz, P. Frinking, Basic acoustic properties of microbubbles, Echocardiogr. 19 (2002) 229–240.
[30] S.M. van der Meer, B. Dollet, M.M. Voormolen, C.T. Chin, A. Bouakaz, N. de Jong, M. Versluis, D. Lohse, Microbubble spectroscopy of ultrasound contrast agents, J. Acoust. Soc. Am. 121 (2007) 648–656.
[31] K. Tsiglifis, N.A. Pelekasis, Nonlinear radial oscillations of encapsulated microbubbles subject to ultrasound: The effect of membrane constitutive law, J. Acoust. Soc. Am. 123 (2008) 4059–4070.
[32] K.E. Morgan, J.S. Allen, P.A. Dayton, J.E. Chomas, A.L. Klibanov, K.W. Ferrara, Experimental and theoretical evaluation of microbubble behavior: effect of transmitted phase and bubble size, IEEE Trans. Ultrason. Ferroelectr. Freq. Control 47 (2000) 1494–1509.

[33] A.A. Doinikov, J.F. Haac, P.A. Dayton, Modeling of nonlinear viscous stress in encapsulating shells of lipid-coated contrast agent microbubbles, Ultrasonics 49 (2009) 269–275.
[34] M. Minnaert, On musical air-bubbles and the sound of running water, Philos. Mag. 16 (1933) 235–248.
[35] T. Wagai, Studies on the foundation and development of diagnostic ultrasound, P. Jpn. Acad. B Phys. 83 (2007) 256–265.
[36] J. McLaughlan, N. Ingram, P.R. Smith, S. Harput, P.L. Coletta, S. Evans, S. Freear, Increasing the sonoporation efficiency of targeted polydisperse microbubble populations using chirp excitation, IEEE Trans. Ultrason. Ferroelectr. Freq. Control 60 (2013) 2511–2520.
[37] K. Chetty, E. Stride, C.A. Sennoga, J.V. Hajnal, R.J. Eckersley, High-speed optical observations and simulation results of SonoVue microbubbles at low-pressure insonation, IEEE Trans. Ultrason. Ferroelectr. Freq. Control 55 (2008) 1333–1342.
[38] C.C. Church, The effects of an elastic solid surface layer on the radial pulsations of gas bubbles, J. Acoust. Soc. Am. 97 (1995) 1510–1521.
[39] K. Sarkar, W.T. Shi, D. Chatterjee, F. Forsberg, Characterization of ultrasound contrast microbubbles using in vitro experiments and viscous and viscoelastic interface models for encapsulation, J. Acoust. Soc. Am. 118 (2005) 539–550.
[40] L. Hoff, P.C. Sontum, J.M. Hovem, Oscillations of polymeric microbubbles: effect of the encapsulating shell, J. Acoust. Soc. Am. 107 (2000) 2272–2280.
[41] P. Marmottant, S. van der Meer, M. Emmer, M. Versluis, N. de Jong, S. Hilgenfeldt, D. Lohse, A model for large amplitude oscillations of coated bubbles accounting for buckling and rupture, J. Acoust. Soc. Am. 118 (2005) 3499–3505.
[42] A.A. Doinikov, P.A. Dayton, Maxwell rheological model for lipid-shelled ultrasound microbubble contrast agents, J. Acoust. Soc. Am. 121 (2007) 3331–3340.
[43] J. Tu, J. Guan, Y. Qiu, T.J. Matula, Estimating the shell parameters of SonoVue microbubbles using light scattering, J. Acoust. Soc. Am. 126 (2009) 2954.
[44] M. Emmer, H. Vos, M. Versluis, N. de Jong, Radial modulation of single microbubbles, IEEE Trans. Ultrason. Ferroelectr. Freq. Control 56 (2009) 2370–2379.
[45] H.J. Vos, M. Emmer, N. de Jong, Oscillation of single microbubbles at room *versus* body temperature, IEEE Ultrasonics symposium, Beijing, China, 2008, pp. 982–984.
[46] P.A. Dayton, J.S. Allen, K.W. Ferrara, The Magnitude of radiation force on ultrasound contrast agents, J. Acoust. Soc. Am. 112 (2002) 2183–2192.
[47] M.A. Borden, G.V. Martinez, J. Ricker, N. Tsvetkova, M. Longo, R.J. Gillies, P.A. Dayton, K.W. Ferrara, Lateral phase separation in lipid-coated microbubbles, Langmuir 22 (2006) 4291–4297.
[48] M. Overvelde, V. Garbin, B. Dollet, N. de Jong, D. Lohse, M. Versluis, Dynamics of coated microbubbles adherent to a wall, Ultrasound Med. Biol. 37 (2011) 1500–1508.
[49] C.F. Caskey, S.M. Stieger, S. Qin, P.A. Dayton, K.W. Ferrara, Direct observations of ultrasound microbubble contrast agent interaction with the microvessel wall, J. Acoust. Soc. Am. 122 (2007) 1191–1200.
[50] D.L. Miller, M.A. Averkiou, A.A. Brayman, E.C. Everbach, C.K. Holland, J.H. Wible, J. Wu, Bioeffects considerations for diagnostic ultrasound contrast agents, J. Ultrasound Med. 27 (2008) 611–632.
[51] K. Kooiman, M.R. Böhmer, M. Emmer, H.J. Vos, C. Chlon, W.T. Shi, C.S. Hall, S.H. de Winter, K. Schroen, M. Versluis, N. de Jong, A. van Wamel, Oil-filled polymer microcapsules for ultrasound-mediated delivery of lipophilic drugs, J. Control. Release 133 (2009) 109–118.
[52] V. Bjerknes, Fields of Force, Columbia University Press, New York, 1906.
[53] H.J. Vos, F. Guidi, E. Boni, P. Tortoli, Method for microbubble characterization using primary radiation force, IEEE Trans. Ultrason. Ferroelectr. Freq. Control 54 (2007) 1333–1345.
[54] P. Marmottant, M. Versluis, N. de Jong, S. Hilgenfeldt, D. Lohse, High-speed imaging of an ultrasound-driven bubble in contact with a wall: "Narcissus" effect and resolved acoustic streaming, Exp. Fluids (2005), http://dx.doi.org/10.1007/s00348-00005-00080-y.
[55] H.J. Vos, B. Dollet, M. Versluis, N. de Jong, Nonspherical shape oscillations of coated microbubbles in contact with a wall, Ultrasound Med. Biol. 37 (2011) 935–948.
[56] M.A.B.. Postema, A. Van Wamel, C.T. Lancée, N. de Jong, Ultrasound-induced encapsulated microbubble phenomena, Ultrasound Med. Biol. 30 (2004) 827–840.
[57] A.A. Doinikov, S. Zhao, P.A. Dayton, Modeling of the acoustic response from contrast agent microbubbles near a rigid wall, Ultrasonics 49 (2009) 195–201.
[58] N. de Jong, L. Hoff, T. Skotland, N. Bom, Absorption and scatter of encapsulated gas filled microspheres: theoretical considerations and some measurements, Ultrasonics 30 (1992) 95–103.
[59] F. Guidi, H.J. Vos, R. Mori, N. de Jong, P. Tortoli, Microbubble characterization through acoustically induced deflation, IEEE Trans. Ultrason. Ferroelectr. Freq. Control 57 (2010) 193–202.
[60] J. Sijl, H.J. Vos, T. Rozendal, N. de Jong, D. Lohse, M. Versluis, Combined optical and acoustical detection of single microbubble dynamics, J. Acoust. Soc. Am. 130 (2011) 3271–3281.
[61] D. Maresca, M. Emmer, P.L.M.J. van Neer, H.J. Vos, M. Versluis, M. Muller, N. de Jong, A.F.W. van der Steen, Acoustic sizing of an ultrasound contrast agent, Ultrasound Med. Biol. 36 (2010) 1713–1721.
[62] K. Kuribayashi, N. Kudo, M. Natori, K. Yamamoto, A high-magnification and high-speed system for the observation of microbubbles under ultrasound exposure, IEEE Ultrasonics symposium, Lake Tahoe, Nevada, 1999, pp. 1755–1758.
[63] C.T. Chin, C.T. Lancée, J.M.G. Borsboom, F. Mastik, M.E. Frijlink, N. de Jong, M. Versluis, D. Lohse, Brandaris 128: A 25 million frames per second digital camera with 128 highly sensitive frames, Rev. Sci. Instrum. 74 (2003) 5026–5034.
[64] E.C. Gelderblom, H.J. Vos, F. Mastik, T. Faez, Y. Luan, T.J. Kokhuis, A.F. van der Steen, D. Lohse, N. de Jong M, M. Versluis, Brandaris 128 ultra-high-speed imaging facility: 10 years of operation, updates, and enhanced features, Rev. Sci. Instrum. 83 (2012) (103706-103706-103711).
[65] X. Chen, J. Wang, M. Versluis, N. de Jong, F.S. Villanueva, Ultra-fast bright field and fluorescence imaging of the dynamics of micrometer-sized objects, Rev. Sci. Instrum. 84 (2013) 063701.
[66] G. Pu, M.A. Borden, M.L. Longo, Collapse and shedding transitions in binary lipid monolayers coating microbubbles, Langmuir 22 (2006) 2993–2999.
[67] M. Emmer, A. van Wamel, D.E. Goertz, N. de Jong, The onset of microbubble vibration, Ultrasound Med. Biol. 33 (2007) 941–949.
[68] M. Overvelde, V. Garbin, J. Sijl, B. Dollet, N. de Jong, D. Lohse, M. Versluis, Nonlinear shell behavior of phospholipid-coated microbubbles, Ultrasound Med. Biol. 36 (2010) 2080–2092.
[69] D.E. Goertz, N. de Jong, A.F.W. van der Steen, Attenuation and size distribution measurements of Definity and manipulated Definity populations, Ultrasound Med. Biol. 33 (2007) 1376–1388.
[70] N. de Jong, R. Cornet, C. Lancée, Higher harmonics of vibrating gas-filled microspheres. Part two: measurements, Ultrasonics 32 (1994) 455–459.
[71] A. Eller, H.G. Flynn, Generation of subharmonics of order one-half by bubbles in a sound field, J. Acoust. Soc. Am. 46 (1969) 727–772.
[72] A. Prosperetti, Nonlinear oscillations of gas bubbles in liquids: transient solutions and the connection between subharmonic signal and cavitation, J. Acoust. Soc. Am. 57 (1975) 810–821.
[73] J. Sijl, B. Dollet, M. Overvelde, V. Garbin, T. Rozendal, N. de Jong, D. Lohse, M. Versluis, Subharmonic behavior of phospholipid-coated ultrasound contrast agent microbubbles, J. Acoust. Soc. Am. 128 (2010) 3239.
[74] N. de Jong, M. Emmer, C.T. Chin, A. Bouakaz, F. Mastik, D. Lohse, M. Versluis, "Compression-only" behavior of phospholipid-coated contrast bubbles, Ultrasound Med. Biol. 33 (2007) 653–656.
[75] B. Dollet, S.M. Van der Meer, V. Garbin, N. de Jong, D. Lohse, M. Versluis, Nonspherical oscillations of ultrasound contrast agent microbubbles, Ultrasound Med. Biol. 34 (2008) 1465–1473.
[76] S.W. Fong, E. Klaseboer, C.K. Turangan, B.C. Khoo, K.C. Hung, Numerical Analysis of a gas bubble near bio-materials in an ultrasound field, Ultrasound Med. Biol. 32 (2006) 925–942.
[77] S. Zhao, K.W. Ferrara, P.A. Dayton, Asymmetric oscillation of adherent targeted ultrasound contrast agents, Appl. Phys. Lett. 87 (2005) (ref. 134103).
[78] P. Prentice, A. Cuschieri, K. Dholakia, M. Prausnitz, P. Campbell, Membrane disruption by optically controlled microbubble cavitation, Nat. Phys. 1 (2005) 107–110.
[79] J.R. Blake, B.B. Taib, G. Doherty, Transient cavities near boundaries. Part 1. Rigid boundary, J. Fluid Mech. 170 (1986) 479–497.
[80] H.J. Vos, B. Dollet, J.G. Bosch, M. Versluis, N. de Jong, Nonspherical vibrations of microbubbles in contact with a wall — a pilot study at low mechanical index, Ultrasound Med. Biol. 34 (2008) 685–688.
[81] P. Marmottant, S. Hilgenfeldt, Controlled vesicle deformation and lysis by single oscillating bubbles, Nature 423 (2003) 153–156.
[82] D.J. May, J.S. Allen, K.W. Ferrara, Dynamics and fragmentation of thick-shelled microbubbles, IEEE Trans. Ultrason. Ferroelectr. Freq. Control 49 (2002) 1400–1410.
[83] J.E. Chomas, P.A. Dayton, J.S. Allen, K.E. Morgan, K.W. Ferrara, Mechanisms of contrast agent destruction, IEEE Trans. Ultrason. Ferroelectr. Freq. Control 48 (2001) 232–248.
[84] R. Tögel, S. Luther, D. Lohse, Viscosity Destablizes Sonoluminescing Bubbles, University of Twente, The Netherlands, 2005.
[85] S. Putterman, K. Weninger, Sonoluminescence: how bubbles turn sound into light, Annu. Rev. Fluid Mech. 32 (2000) 445–476.
[86] M. Versluis, B. Schmitz, A. von der Heydt, D. Lohse, How snapping shrimp snap: through cavitating bubbles, Science 289 (2000) 2114–2117.
[87] D.M. Hallow, A.D. Mahajan, T.E. McCutchen, M.R. Prausnitz, Measurement and correlation of acoustic cavitation with cellular bioeffects, Ultrasound Med. Biol. 32 (2006) 1111–1122.
[88] C.C. Coussios, R.A. Roy, Applications of acoustics and cavitation to noninvasive therapy and drug delivery, Annu. Rev. Fluid Mech. 40 (2008) 395–420.
[89] M.S. Plesset, T.P. Mitchell, On the Stability of the Spherical Shape of a Vapor Cavity in a Liquid, Quarterly Appl. Math. 12 (4) (1956).
[90] J.E. Chomas, P. Dayton, D. May, K. Ferrara, Threshold of fragmentation for ultrasonic contrast agents, J. Biomed. Opt. 6 (2001) 141–150.
[91] N. de Jong, M. Emmer, A. van Wamel, M. Versluis, Ultrasonic characterization of ultrasound contrast agents, Med. Biol. Eng. Comput. 47 (2009) 861–873.
[92] P. Marmottant, A. Bouakaz, N. de Jong, C. Quilliet, Buckling resistance of solid shell bubbles under ultrasound, J. Acoust. Soc. Am. 129 (2011) 1231–1239.
[93] D. Lensen, E.C. Gelderblom, D.M. Vriezema, P. Marmottant, N. Verdonschot, M. Versluis, N. de Jong, J.C. Van Hest, Biodegradable polymeric microcapsules for selective ultrasound-triggered drug release, Soft Matter 7 (2011) 5417–5422.
[94] A. Bouakaz, M. Versluis, N. de Jong, High-speed optical observations of contrast agent destruction, Ultrasound Med. Biol. 31 (2005) 391–399.
[95] A. van Wamel, K. Kooiman, M. Harteveld, M. Emmer, F.J. Ten Cate, M. Versluis, N. de Jong, Vibrating microbubbles poking individual cells: drug transfer into cells via sonoporation, J. Control. Release 112 (2006) 149–155.
[96] J.A. Rooney, Hemolysis near an ultrasonically pulsating gas bubble, Science 169 (1970) 869–871.
[97] S.A. Elder, Cavitation microstreaming, J. Acoust. Soc. Am. 31 (1959) 54–64.
[98] J. Collis, R. Manasseh, P. Liovic, P. Tho, A. Ooi, K. Petkovic-Duran, Y. Zhu, Cavitation microstreaming and stress fields created by microbubbles, Ultrasonics 50 (2010) 273–279.
[99] E.C. Gelderblom, Ultra-High-Speed Fluorescence Imaging, Universiteit Twente, 2012.
[100] M.M. Forbes, W.D. O'Brien Jr., Development of a theoretical model describing sonoporation activity of cells exposed to ultrasound in the presence of contrast agents, J. Acoust. Soc. Am. 131 (2012) 2723–2729.

[101] A.A. Doinikov, A. Bouakaz, Theoretical investigation of shear stress generated by a contrast microbubble on the cell membrane as a mechanism for sonoporation, J. Acoust. Soc. Am. 128 (2010) 11–19.
[102] J. Wu, Theoretical study on shear stress generated by microstreaming surrounding contrast agents attached to living cells, Ultrasound Med. Biol. 28 (2002) 125–129.
[103] R. Dijkink, C.-D. Ohl, Measurement of cavitation induced wall shear stress, Appl. Phys. Lett. 93 (2008) (254107-254107-254103).
[104] A.M. Malek, S.L. Alper, S. Izumo, Hemodynamic shear stress and its role in atherosclerosis, JAMA 282 (1999) 2035–2042.
[105] C.-D. Ohl, M. Arora, R. Ikink, N. de Jong, M. Versluis, M. Delius, D. Lohse, Sonoporation from jetting cavitation bubbles, Biophys. J. 91 (2006) 4285–4295.
[106] E.-A. Brujan, K. Nahen, P. Schmidt, A. Vogel, Dynamics of laser-induced cavitation bubbles near elastic boundaries: influence of the elastic modulus, J. Fluid Mech. 433 (2001) 283–314.
[107] H. Chen, W. Kreider, A.A. Brayman, M.R. Bailey, T.J. Matula, Blood vessel deformations on microsecond time scales by ultrasonic cavitation, Phys. Rev. Lett. 106 (2011) 034301.
[108] V. Garbin, D. Cojoc, E. Ferrari, E. Di Fabrizio, M.L.J. Overvelde, S.M. van der Meer, N. de Jong, D. Lohse, M. Versluis, Changes in microbubble dynamics near a boundary revealed by combined optical micromanipulation and high-speed imaging, Appl. Phys. Lett. 90 (2007) 114103.
[109] A.A. Doinikov, L. Aired, A. Bouakaz, Acoustic response from a bubble pulsating near a fluid layer of finite density and thickness, J. Acoust. Soc. Am. 129 (2011) 616–621.
[110] T.A. Hay, Y.A. Ilinskii, E.A. Zabolotskaya, M.F. Hamilton, Model for bubble pulsation in liquid between parallel viscoelastic layers, J. Acoust. Soc. Am. 132 (2012) 124.
[111] T. Leighton, The inertial terms in equations of motion for bubbles in tubular vessels or between plates, J. Acoust. Soc. Am. 130 (2011) 3333–3338.
[112] D.H. Thomas, V. Sboros, M. Emmer, H. Vos, N. de Jong, Microbubble oscillations in capillary tubes, IEEE Trans. Ultrason. Ferroelectr. Freq. Control 60 (2013) 105–114.
[113] T. Faez, I. Skachkov, M. Versluis, K. Kooiman, N. de Jong, *In vivo* characterization of ultrasound contrast agents: microbubble spectroscopy in a chicken embryo, Ultrasound Med. Biol. 38 (2012) 1608–1617.
[114] S. Bao, B.D. Thrall, D.L. Miller, Transfection of a reporter plasmid into cultured cells by sonoporation in vitro, Ultrasound Med. Biol. 23 (1997) 953–959.
[115] S. Kotopoulis, G. Dimcevski, O.H. Gilja, D. Hoem, M. Postema, Treatment of human pancreatic cancer using combined ultrasound, microbubbles, and gemcitabine: a clinical case study, Med. Phys. 40 (2013) 072902.
[116] C.Y. Lai, C.H. Wu, C.C. Chen, P.C. Li, Quantitative relations of acoustic inertial cavitation with sonoporation and cell viability, Ultrasound Med. Biol. 32 (2006) 1931–1941.
[117] Y. Qiu, Y. Luo, Y. Zhang, W. Cui, D. Zhang, J. Wu, J. Zhang, J. Tu, The correlation between acoustic cavitation and sonoporation involved in ultrasound-mediated DNA transfection with polyethylenimine (PEI) in vitro, J. Control. Release 145 (2010) 40–48.
[118] M.M. Forbes, R.L. Steinberg, W.D. O'Brien Jr., Examination of inertial cavitation of Optison in producing sonoporation of chinese hamster ovary cells, Ultrasound Med. Biol. 34 (2008) 2009–2018.
[119] M. Kinoshita, K. Hynynen, Key factors that affect sonoporation efficiency in in vitro settings: the importance of standing wave in sonoporation, Biochem. Biophys. Res. Commun. 359 (2007) 860–865.
[120] A. Delalande, S. Kotopoulis, T. Rovers, C. Pichon, M. Postema, Sonoporation at a low mechanical index, Bubble Sci. Eng. Technol. 3 (2011) 3–12.
[121] Y. Hu, J.M.F. Wan, A.C.H. Yu, Membrane perforation and recovery dynamics in microbubble-mediated sonoporation, Ultrasound Med. Biol. 39 (2013) 2393–2405.
[122] B. Krasovitski, V. Frenkel, S. Shoham, E. Kimmel, Intramembrane cavitation as a unifying mechanism for ultrasound-induced bioeffects, Proc. Natl. Acad. Sci. U. S. A. 108 (2011) 3258–3263.
[123] S.P. Wrenn, E. Small, N. Dan, Bubble nucleation in lipid bilayers: a mechanism for low frequency ultrasound disruption, Biochim. Biophys. Acta 1828 (2013) 1192–1197.
[124] S.M. Rappaport, A.M. Berezhkovskii, J. Zimmerberg, S.M. Bezrukov, Thermodynamics of interleaflet cavitation in lipid bilayer membranes, Phys. Rev. E Stat. Nonlinear Soft Matter Phys. 87 (2013) 022715.
[125] E.C. Pua, P. Zhong, Ultrasound-mediated drug delivery, IEEE Eng. Med. Biol. Mag. 28 (2009) 64–75.
[126] R. Karshafian, P.D. Bevan, R. Williams, S. Samac, P.N. Burns, Sonoporation by ultrasound-activated microbubble contrast agents: effect of acoustic exposure parameters on cell membrane permeability and cell viability, Ultrasound Med. Biol. 35 (2009) 847–860.
[127] R.K. Schlicher, H. Radhakrishna, T.P. Tolentino, R.P. Apkarian, V. Zarnitsyn, M.R. Prausnitz, Mechanism of intracellular delivery by acoustic cavitation, Ultrasound Med. Biol. 32 (2006) 915–924.
[128] B.D. Meijering, L.J. Juffermans, A. van Wamel, R.H. Henning, I.S. Zuhorn, M. Emmer, A.M. Versteilen, W. Paulus, W.H. van Gilst, K. Kooiman, N. de Jong, R.J. Musters, L.E. Deelman, O. Kamp, Ultrasound and microbubble-targeted delivery of macromolecules is regulated by induction of endocytosis and pore formation, Circ. Res. 104 (2009) 679–687.
[129] X. Chen, J.M. Wan, A.C. Yu, Sonoporation as a cellular stress: induction of morphological repression and developmental delays, Ultrasound Med. Biol. 39 (2013) 1075–1086.
[130] S. Mehier-Humbert, T. Bettinger, F. Yan, R.H. Guy, Plasma membrane poration induced by ultrasound exposure: Implication for drug delivery, J. Control. Release 104 (2005) 213–222.
[131] Y. Zhou, J.M. Cui, C.X. Deng, Dynamics of sonoporation correlated with acoustic cavitation activities, Biophys. J. 94 (2008) L51–L53.
[132] T.A. Tran, S. Roger, J.Y. Le Guennec, F. Tranquart, A. Bouakaz, Effect of ultrasound-activated microbubbles on the cell electrophysiological properties, Ultrasound Med. Biol. 33 (2007) 158–163.
[133] B.D.M. Meijering, R.H. Henning, W.H. van Gilst, I. Gavrilovic, A. van Wamel, L.E. Deelman, Optimization of ultrasound and microbubbles targeted gene delivery to cultured primary endothelial cells, J. Drug Target. 15 (2007) 664–671.
[134] A. van Wamel, A. Bouakaz, M. Versluis, N. de Jong, Micromanipulation of endothelial cells: ultrasound-microbubble-cell interaction, Ultrasound Med. Biol. 30 (2004) 1255–1258.
[135] N. Kudo, K. Okada, K. Yamamoto, Sonoporation by single-shot pulsed ultrasound with microbubbles adjacent to cells, Biophys. J. 96 (2009) 4866–4876.
[136] N. Sheikov, N. McDannold, S. Sharma, K. Hynynen, Effect of focused ultrasound applied with an ultrasound contrast agent on the tight junctional integrity of the brain microvascular endothelium, Ultrasound Med. Biol. 34 (2008) 1093–1104.
[137] Y. Liu, S. Yi, J. Zhang, Z. Fang, F. Zhou, W. Jia, Z. Liu, G. Ye, Effect of microbubble-enhanced ultrasound on prostate permeability: a potential therapeutic method for prostate disease, Urology 81 (2013) e921–e927 (921).
[138] Z. Fan, H. Liu, M. Mayer, C.X. Deng, Spatiotemporally controlled single cell sonoporation, Proc. Natl. Acad. Sci. U. S. A. 109 (2012) 16486–16491.
[139] F. Yang, N. Gu, D. Chen, X. Xi, D. Zhang, Y. Li, J. Wu, Experimental study on cell self-sealing during sonoporation, J. Control. Release 131 (2008) 205–210.
[140] L.F. Jin, F. Li, H.P. Wang, F. Wei, P. Qin, L.F. Du, Ultrasound targeted microbubble destruction stimulates cellular endocytosis in facilitation of adeno-associated virus delivery, Int. J. Mol. Sci. 14 (2013) 9737–9750.
[141] T. Sundqvist, S.M. Liu, Hydrogen peroxide stimulates endocytosis in cultured bovine aortic endothelial cells, Acta Physiol. Scand. 149 (1993) 127–131.
[142] P.E. MacDonald, L. Eliasson, P. Rorsman, Calcium increases endocytotic vesicle size and accelerates membrane fission in insulin-secreting INS-1 cells, J. Cell Sci. 118 (2005) 5911–5920.
[143] J. Saliez, C. Bouzin, G. Rath, P. Ghisdal, F. Desjardins, R. Rezzani, L.F. Rodella, J. Vriens, B. Nilius, O. Feron, J.L. Balligand, C. Dessy, Role of caveolar compartmentation in endothelium-derived hyperpolarizing factor-mediated relaxation: Ca2+ signals and gap junction function are regulated by caveolin in endothelial cells, Circulation 117 (2008) 1065–1074.
[144] Z. Fan, R.E. Kumon, J. Park, C.X. Deng, Intracellular delivery and calcium transients generated in sonoporation facilitated by microbubbles, J. Control. Release 142 (2010) 31–39.
[145] L.J. Juffermans, A. van Dijk, C.A. Jongenelen, B. Drukarch, A. Reijerkerk, H.E. de Vries, O. Kamp, R.J. Musters, Ultrasound and microbubble-induced intra- and intercellular bioeffects in primary endothelial cells, Ultrasound Med. Biol. 35 (2009) 1917–1927.
[146] L.J. Juffermans, P.A. Dijkmans, R.J. Musters, C.A. Visser, O. Kamp, Transient permeabilization of cell membranes by ultrasound-exposed microbubbles is related to formation of hydrogen peroxide, Am. J. Physiol. Heart Circ. Physiol. 291 (2006) H1595–H1601.
[147] T.A. Tran, J.Y. Le Guennec, P. Bougnoux, F. Tranquart, A. Bouakaz, Characterization of cell membrane response to ultrasound activated microbubbles, IEEE Trans. Ultrason. Ferroelectr. Freq. Control 55 (2008) 44–49.
[148] L.J. Juffermans, O. Kamp, P.A. Dijkmans, C.A. Visser, R.J. Musters, Low-intensity ultrasound-exposed microbubbles provoke local hyperpolarization of the cell membrane via activation of BK(Ca) channels, Ultrasound Med. Biol. 34 (2008) 502–508.
[149] A.C. Guyton, J.E. Hall, Medical Physiology, Elsevier Saunders, London, 2006.
[150] R.E. Kumon, M. Aehle, D. Sabens, P. Parikh, Y.W. Han, D. Kourennyi, C.X. Deng, Spatiotemporal effects of sonoporation measured by real-time calcium imaging, Ultrasound Med. Biol. 35 (2009) 494–506.
[151] P.F. Davies, Flow-mediated endothelial mechanotransduction, Physiol. Rev. 75 (1995) 519–560.
[152] B. Nilius, G. Droogmans, R. Wondergem, Transient receptor potential channels in endothelium: solving the calcium entry puzzle? Endothelium 10 (2003) 5–15.
[153] G. Apodaca, Modulation of membrane traffic by mechanical stimuli, Am. J. Physiol. Ren. Physiol. 282 (2002) F179–F190.
[154] K. Niwa, J. Sakai, T. Karino, H. Aonuma, T. Watanabe, T. Ohyama, O. Inanami, M. Kuwabara, Reactive oxygen species mediate shear stress-induced fluid-phase endocytosis in vascular endothelial cells, Free Radic. Res. 40 (2006) 167–174.
[155] A. Yudina, C.T.W. Moonen Lepetit-Coiffé, Evaluation of the temporal windown for drug delivery following ultrasound-mediated membrane permeability enhancement, Mol. Imaging Biol. 13 (2011) 239–249.
[156] K. Kooiman, M. Emmer, M. Foppen-Harteveld, A. van Wamel, N. de Jong, Increasing the endothelial layer permeability through ultrasound-activated microbubbles, IEEE Trans. Biomed. Eng. 57 (2010) 29–32.
[157] K. Kooiman, A.F.W. van der Steen, N. de Jong, Role of intracellular calcium and reactive oxygen species in microbubble-mediated alterations of endothelial layer permeability, IEEE Trans. Ultrason. Ferroelectr. Freq. Control 60 (2013) 1811–1815.
[158] D.C. Walker, A. MacKenzie, S. Hosford, The structure of the tricellular region of endothelial tight junctions of pulmonary capillaries analyzed by freeze-fracture, Microvasc. Res. 48 (1994) 259–281.
[159] A.R. Burns, D.C. Walker, E.S. Brown, L.T. Thurmon, R.A. Bowden, C.R. Keese, S.I. Simon, M.L. Entman, C.W. Smith, Neutrophil transendothelial migration is independent of tight junctions and occurs preferentially at tricellular corners, J. Immunol. 159 (1997) 2893–2903.
[160] M. Ushio-Fukai, R.S. Frey, T. Fukai, A.B.. Malik, Reactive oxygen species and endothelial permeability, Free Radical Effects on Membranes, Elsevier Academic Press Inc., San Diego, 2008, pp. 147–189.
[161] K.G. Birukov, Cyclic stretch, reactive oxygen species, and vascular remodeling, Antioxid. Redox Signal. 11 (2009) 1651–1667.
[162] D. Mehta, A.B.. Malik, Signaling mechanisms regulating endothelial permeability, Physiol. Rev. 86 (2006) 279–367.
[163] K. Kooiman, M. Foppen-Harteveld, A.F.W. van der Steen, N. de Jong, Sonoporation of endothelial cells by vibrating targeted microbubbles, J. Control. Release 154 (2011) 35–41.

[164] J.R. Lindner, Molecular imaging of cardiovascular disease with contrast-enhanced ultrasonography, Nat. Rev. Cardiol. 6 (2009) 475–481.
[165] F.W. Mauldin Jr., A.H. Dhanaliwala, A.V. Patil, J.A. Hossack, Real-time targeted molecular imaging using singular value spectra properties to isolate the adherent microbubble signal, Phys. Med. Biol. 57 (2012) 5275–5293.
[166] A. Needles, O. Couture, F.S. Foster, A method for differentiating targeted microbubbles in real time using subharmonic micro-ultrasound and interframe filtering, Ultrasound Med. Biol. 35 (2009) 1564–1573.
[167] S. Zhao, D.E. Kruse, K.W. Ferrara, P.A. Dayton, Acoustic response from adherent targeted contrast agents, J. Acoust. Soc. Am. 120 (2006) EL63–EL69.
[168] J.M. Escoffre, J. Piron, A. Novell, A. Bouakaz, Doxorubicin delivery into tumor cells with ultrasound and microbubbles, Mol. Pharm. 8 (2011) 799–806.
[169] A. Sternberg, M. Amar, R. Alfici, G. Groisman, Conclusions from a study of venous invasion in stage IV colorectal adenocarcinoma, J. Clin. Pathol. 55 (2002) 17–21.
[170] S. Eguchi, M. Takatsuki, M. Hidaka, A. Soyama, T. Tomonaga, I. Muraoka, T. Kanematsu, Predictor for histological microvascular invasion of hepatocellular carcinoma: a lesson from 229 consecutive cases of curative liver resection, World J. Surg. 34 (2010) 1034–1038.
[171] S. Chang, J. Guo, J. Sun, S. Zhu, Y. Yan, Y. Zhu, M. Li, Z. Wang, R.X. Xu, Targeted microbubbles for ultrasound mediated gene transfection and apoptosis induction in ovarian cancer cells, Ultrason. Sonochem. 20 (2013) 171–179.
[172] P.P. Cagol, E. Pasqual, S. Bacchetti, Natural history of the neoplastic locoregional disease: clinical and pathological patterns, J. Exp. Clin. Cancer Res. 22 (2003) 1–4.
[173] A. Delalande, A. Bouakaz, G. Renault, F. Tabareau, S. Kotopoulis, P. Midoux, B. Arbeille, R. Uzbekov, S. Chakravarti, M. Postema, C. Pichon, Ultrasound and microbubble-assisted gene delivery in Achilles tendons: long lasting gene expression and restoration of fibromodulin KO phenotype, J. Control. Release 156 (2011) 223–230.
[174] J. Park, Z. Fan, C.X. Deng, Effects of shear stress cultivation on cell membrane disruption and intracellular calcium concentration in sonoporation of endothelial cells, J. Biomech. 44 (2011) 164–169.
[175] S. Mehier-Humbert, F. Yan, P. Frinking, M. Schneider, R.H. Guy, T. Bettinger, Ultrasound-mediated gene delivery: influence of contrast agent on transfection, Bioconjug. Chem. 18 (2007) 652–662.
[176] M. Cochran, M.A. Wheatley, In vitro gene delivery with ultrasound-triggered polymer microbubbles, Ultrasound Med. Biol. 39 (2013) 1102–1119.
[177] M.R. Böhmer, C.H.T. Chlon, B.I. Raju, C.T. Chin, T. Shevchenko, A.L. Klibanov, Focused ultrasound and microbubbles for enhanced extravasation, J. Control. Release 148 (2010) 18–24.
[178] Y. Zhang, R. Tachibana, A. Okamoto, T. Azuma, A. Sasaki, K. Yoshinaka, Y. Tei, S. Takagi, Y. Matsumoto, Ultrasound-mediated gene transfection in vitro: effect of ultrasonic parameters on efficiency and cell viability, Int. J. Hyperth. 28 (2012) 290–299.
[179] L.C. Phillips, A.L. Klibanov, B.R. Wamhoff, J.A. Hossack, Localized ultrasound enhances delivery of rapamycin from microbubbles to prevent smooth muscle proliferation, J. Control. Release 154 (2011) 42–49.
[180] L.C. Phillips, A.L. Klibanov, B.R. Wamhoff, J.A. Hossack, Targeted gene transfection from microbubbles into vascular smooth muscle cells using focused, ultrasound-mediated delivery, Ultrasound Med. Biol. 36 (2010) 1470–1480.
[181] S. Chen, R.V. Shohet, R. Bekeredjian, P. Frenkel, P.A. Grayburn, Optimization of ultrasound parameters for cardiac gene delivery of adenoviral or plasmid deoxyribonucleic acid by ultrasound-targeted microbubble destruction, J. Am. Coll. Cardiol. 42 (2003) 301–308.
[182] E.C. Unger, T.P. McCreery, R.H. Sweitzer, V.E. Caldwell, Y. Wu, Acoustically active lipospheres containing paclitaxel: a new therapeutic ultrasound contrast agent, Invest. Radiol. 33 (1998) 886–892.
[183] M.S. Tartis, J. McCallan, A.F.H. Lum, R. LaBell, S.M. Stieger, T.O. Matsunaga, K.W. Ferrara, Therapeutic effects of paclitaxel-containing ultrasound contrast agents, Ultrasound Med. Biol. 32 (2006) 1771–1780.
[184] M.J. Shortencarier, P.A. Dayton, S.H. Bloch, P.A. Schumann, T.O. Matsunaga, K. W. Ferrara, A method for radiation-force localized drug delivery using gas-filled lipospheres, IEEE Trans. Ultrason. Ferroelectr. Freq. Control 51 (2004) 822–831.
[185] A. Kheirolomoom, P.A. Dayton, A.F. Lum, E. Little, E.E. Paoli, H. Zheng, K.W. Ferrara, Acoustically-active microbubbles conjugated to liposomes: characterization of a proposed drug delivery vehicle, J. Control. Release 118 (2007) 275–284.
[186] Y. Luan, T. Faez, E. Gelderblom, I. Skachkov, B. Geers, I. Lentacker, T. van der Steen, M. Versluis, N. de Jong, Acoustical properties of individual liposome-loaded microbubbles, Ultrasound Med. Biol. 38 (2012) 2174–2185.
[187] J. McLaughlan, N. Ingram, R. Abou-Saleh, S. Harput, T. Evans, S. Evens, L. Coletta, S. Freear, High-frequency subharmonic imaging of liposome-loaded microbubbles, IEEE Ultrasonics Symposium Proceedings, Czech Republic, Prague, 2013, (IUS1-PC3-2).
[188] Y. Luan, G. Lajoinie, E. Gelderblom, I. Skachkov, H. Dewitte, I. Lentacker, T. van Rooij, H.J. Vos, A.F.W. van der Steen, M. Versluis, N. de Jong, Liposome shedding from a vibrating microbubble on nanoseconds timescale, IEEE Ultrasonics Symposium Proceedings, Czech Republic, Prague, 2013, (IUS1-B1-2).
[189] J.L. Tlaxca, J.J. Rychak, P.B. Ernst, P.R. Konkalmatt, T.I. Shevchenko, T.T. Pizzaro, J. Rivera-Nieves, A.L. Klibanov, M.B. Lawrence, Ultrasound-based molecular imaging and specific gene delivery to mesenteric vasculature by endothelial adhesion molecule targeted microbubbles in a mouse model of Crohn's disease, J. Control. Release 165 (2013) 216–225.
[190] A. Xie, T. Belcik, Y. Qi, T.K. Morgan, S.A. Champaneri, S. Taylor, B.P. Davidson, Y. Zhao, A.L. Klibanov, M.A. Kuliszewski, H. Leong-Poi, A. Ammi, J.R. Lindner, Ultrasound-mediated vascular gene transfection by cavitation of endothelial-targeted cationic microbubbles, Jacc Cardiovasc. Imaging 5 (2012) 1253–1262.
[191] L.C. Phillips, A.L. Klibanov, B.R. Wamhoff, J.A. Hossack, Intravascular ultrasound detection and delivery of molecularly targeted microbubbles for gene delivery, IEEE Trans. Ultrason. Ferroelectr. Freq. Control 59 (2012) 1596–1601.
[192] C.H. Fan, C.Y. Ting, H.L. Liu, C.Y. Huang, H.Y. Hsieh, T.C. Yen, K.C. Wei, C.K. Yeh, Antiangiogenic-targeting drug-loaded microbubbles combined with focused ultrasound for glioma treatment, Biomaterials 34 (2013) 2142–2155.
[193] A.F. Lum, M.A. Borden, P.A. Dayton, D.E. Kruse, S.I. Simon, K.W. Ferrara, Ultrasound radiation force enables targeted deposition of model drug carriers loaded on microbubbles, J. Control. Release 111 (2006) 128–134.
[194] I. Lentacker, S.C. de Smedt, J. Demeester, V. van Marck, M. Bracke, N.N. Sanders, Lipoplex-loaded microbubbles for gene delivery: a Trojan horse controlled by ultrasound, Adv. Funct. Mater. 17 (2007) 1910–1916.
[195] I. Lentacker, B. Geers, J. Demeester, S.C. de Smedt, N.N. Sanders, Design and evaluation of doxorubicin-containing microbubbles for ultrasound-triggered doxorubicin delivery: cytotoxicity and mechanisms involved, Mol. Ther. 18 (2010) 101–108.
[196] B. Geers, I. Lentacker, N.N. Sanders, J. Demeester, S. Meairs, S.C. De Smedt, Self-assembled liposome-loaded microbubbles: the missing link for safe and efficient ultrasound triggered drug-delivery, J. Control. Release 152 (2011) 249–256.
[197] D. Yang, Y.H. Gao, K.B. Tan, Z.X. Zuo, W.X. Yang, X. Hua, P.J. Li, Y. Zhang, G. Wang, Inhibition of hepatic fibrosis with artificial microRNA using ultrasound and cationic liposome-bearing microbubbles, Gene Ther. 20 (2013) 1140–1148.
[198] A.L. Klibanov, T.I. Shevchenko, B.I. Raju, R. Seip, C.T. Chin, Ultrasound-triggered release of materials entrapped in microbubble-liposome constructs: a tool for targeted drug delivery, J. Control. Release 148 (2010) 13–17.
[199] M.A. Borden, C.F. Caskey, E. Little, R.J. Gillies, K.W. Ferrara, DNA and polylysine adsorption and multilayer construction onto cationic lipid-coated microbubbles, Langmuir 23 (2007) 9401–9408.
[200] J.P. Christiansen, B.A. French, A.L. Klibanov, S. Kaul, J.R. Lindner, Targeted tissue transfection with ultrasound destruction of plasmid-bearing cationic microbubbles, Ultrasound Med. Biol. 29 (2003) 1759–1767.
[201] M. Vannan, T. McCreery, P. Li, Z. Han, E. Unger, B. Kuersten, E. Nabel, S. Rajagopalan, Ultrasound-mediated transfection of canine myocardium by intravenous administration of cationic microbubble-linked plasmid DNA, J. Am. Soc. Echocardiogr. 15 (2002) 214–218.
[202] A.R. Carson, C.F. McTiernan, L. Lavery, A. Hodnick, M. Grata, X. Leng, J. Wang, X. Chen, R.A. Modzelewski, F.S. Villanueva, Gene therapy of carcinoma using ultrasound-targeted microbubble destruction, Ultrasound Med. Biol. 37 (2011) 393–402.
[203] T.R. Porter, W.L. Hiser, D. Kricsfeld, U. Deligonul, F. Xie, P. Iversen, S. Radio, Inhibition of carotid artery neointimal formation with intravenous microbubbles, Ultrasound Med. Biol. 27 (2001) 259–265.
[204] Y. Taniyama, K. Tachibana, K. Hiraoka, T. Namba, K. Yamasaki, N. Hashiya, M. Aoki, T. Ogihara, K. Yasufumi, R. Morishita, Local delivery of plasmid DNA into rat carotid artery using ultrasound, Circulation 105 (2002) 1233–1239.
[205] R.V. Shohet, S. Chen, Y.T. Zhou, Z. Wang, R.S. Meidell, R.H. Unger, P.A. Grayburn, Echocardiographic destruction of albumin microbubbles directs gene delivery to the myocardium, Circulation 101 (2000) 2554–2556.
[206] I. Lentacker, B.G. de Geest, R.E. Vandenbroucke, L. Peeters, J. Demeester, S.C. de Smedt, N.N. Sanders, Ultrasound-responsive polymer-coated microbubbles that bind and protect DNA, Langmuir 22 (2006) 7273–7278.
[207] S. Tinkov, G. Winter, C. Coester, R. Bekeredjian, New doxorubicin-loaded phospholipid microbubbles for targeted tumor therapy: Part I–Formulation development and in-vitro characterization, J. Control. Release 143 (2010) 143–150.
[208] J. Kang, X. Wu, Z. Wang, H. Ran, C. Xu, J. Wu, Z. Wang, Y. Zhang, Antitumor effect of docetaxel-loaded lipid microbubbles combined with ultrasound-targeted microbubble activation on VX2 rabbit liver tumors, J. Ultrasound Med. 29 (2010) 61–70.
[209] W. Xing, W.Z. Gang, Z. Yong, Z.Y. Yi, X.C. Shan, R.H. Tao, Treatment of xenografted ovarian carcinoma using paclitaxel-loaded ultrasound microbubbles, Acad. Radiol. 15 (2008) 1574–1579.
[210] P. Li, Y. Zheng, H. Ran, J. Tan, Y. Lin, Q. Zhang, J. Ren, Z. Wang, Ultrasound triggered drug release from 10-hydroxycamptothecin-loaded phospholipid microbubbles for targeted tumor therapy in mice, J. Control. Release 162 (2012) 349–354.
[211] C.Y. Ting, C.H. Fan, H.L. Liu, C.Y. Huang, H.Y. Hsieh, T.C. Yen, K.C. Wei, C.K. Yeh, Concurrent blood–brain barrier opening and local drug delivery using drug-carrying microbubbles and focused ultrasound for brain glioma treatment, Biomaterials 33 (2012) 704–712.
[212] L.C. Phillips, A.H. Dhanaliwala, A.L. Klibanov, J.A. Hossack, B.R. Wamhoff, Focused ultrasound-mediated drug delivery from microbubbles reduces drug dose necessary for therapeutic effect on neointima formation—brief report, Arterioscler. Thromb. Vasc. Biol. 31 (2011) 2853–2855.
[213] A.R. Carson, C.F. McTiernan, L. Lavery, M. Grata, X. Leng, J. Wang, X. Chen, F.S. Villanueva, Ultrasound-targeted microbubble destruction to deliver siRNA cancer therapy, Cancer Res. 72 (2012) 6191–6199.
[214] J. Ren, C. Xu, Z. Zhou, Y. Zhang, X. Li, Y. Zheng, H. Ran, Z. Wang, A novel ultrasound microbubble carrying gene and Tat peptide: preparation and characterization, Acad. Radiol. 16 (2009) 1457–1465.
[215] R. Bekeredjian, S. Chen, P.A. Frenkel, P.A. Grayburn, R.V. Shohet, Ultrasound-targeted microbubble destruction can repeatedly direct highly specific plasmid expression to the heart, Circulation 108 (2003) 1022–1026.
[216] A.H. Liao, Y.K. Li, W.J. Lee, M.F. Wu, H.L. Liu, M.L. Kuo, Estimating the delivery efficiency of drug-loaded microbubbles in cancer cells with ultrasound and bioluminescence imaging, Ultrasound Med. Biol. 38 (2012) 1938–1948.
[217] M.A. Wheatley, M.C. Cochran, J.R. Eisenbrey, K.L. Oum, Cellular signal transduction can be induced by TRAIL conjugated to microcapsules, J. Biomed. Mater. Res. A 100 (2012) 2602–2611.

[218] J.R. Eisenbrey, P. Huang, J. Hsu, M.A. Wheatley, Ultrasound triggered cell death in vitro with doxorubicin loaded poly lactic-acid contrast agents, Ultrasonics 49 (2009) 628–633.
[219] J.R. Eisenbrey, O.M. Burstein, R. Kambhampati, F. Forsberg, J.B. Liu, M.A. Wheatley, Development and optimization of a doxorubicin loaded poly(lactic acid) contrast agent for ultrasound directed drug delivery, J. Control. Release 143 (2010) 38–44.
[220] S. Fokong, B. Theek, Z. Wu, P. Koczera, L. Appold, S. Jorge, U. Resch-Genger, M. van Zandvoort, G. Storm, F. Kiessling, T. Lammers, Image-guided, targeted and triggered drug delivery to tumors using polymer-based microbubbles, J. Control. Release 163 (2012) 75–81.
[221] M.C. Cochran, J. Eisenbrey, R.O. Ouma, M. Soulen, M.A. Wheatley, Doxorubicin and paclitaxel loaded microbubbles for ultrasound triggered drug delivery, Int. J. Pharm. 414 (2011) 161–170.
[222] C. Niu, Z. Wang, G. Lu, T.M. Krupka, Y. Sun, Y. You, W. Song, H. Ran, P. Li, Y. Zheng, Doxorubicin loaded superparamagnetic PLGA-iron oxide multifunctional microbubbles for dual-mode US/MR imaging and therapy of metastasis in lymph nodes, Biomaterials 34 (2013) 2307–2317.
[223] Y. Zheng, Y. Zhang, M. Ao, P. Zhang, H. Zhang, P. Li, L. Qing, Z. Wang, H. Ran, Hematoporphyrin encapsulated PLGA microbubble for contrast enhanced ultrasound imaging and sonodynamic therapy, J. Microencapsul. 29 (2012) 437–444.
[224] S. Seemann, P. Hauff, M. Schultze-Mosgau, C. Lehmann, R. Reszka, Pharmaceutical evaluation of gas-filled microparticles as gene delivery system, Pharm. Res. 19 (2002) 250–257.
[225] M.A. Wheatley, F. Forsberg, K. Oum, R. Ro, D. El-Sherif, Comparison of in vitro and in vivo acoustic response of a novel 50:50 PLGA contrast agent, Ultrasonics 44 (2006) 360–367.
[226] J.R. Eisenbrey, M.C. Soulen, M.A. Wheatley, Delivery of encapsulated doxorubicin by ultrasound-mediated size reduction of drug-loaded polymer contrast agents, IEEE Trans. Biomed. Eng. 57 (2010) 24–28.
[227] H. Maeda, J. Wu, T. Sawa, Y. Matsumura, K. Hori, Tumor vascular permeability and the EPR effect in macromolecular therapeutics: a review, J. Control. Release 65 (2000) 271–284.
[228] J.M. Anderson, M.S. Shive, Biodegradation and biocompatibility of PLA and PLGA microspheres, Adv. Drug Deliv. Rev. 28 (1997) 5–24.
[229] M.C. Cochran, J.R. Eisenbrey, M.C. Soulen, S.M. Schultz, R.O. Ouma, S.B. White, E.E. Furth, M.A. Wheatley, Disposition of ultrasound sensitive polymeric drug carrier in a rat hepatocellular carcinoma model, Acad. Radiol. 18 (2011) 1341–1348.
[230] W.T. Shi, M. Böhmer, A. van Wamel, M. Celebi, A.L. Klibanov, C.T. Chin, C. Chlon, M. Emmer, K. Kooiman, N. de Jong, C.S. Hall, Ultrasound therapy with drug loaded microcapsules, IEEE Ultrasonics Symposium Proceedings, New York, USA, 2007, pp. 773–776.
[231] D.M. Skyba, R.J. Price, A.Z. Linka, T.C. Skalak, S. Kaul, Direct in vivo visualization of intravascular destruction of microbubbles by ultrasound and its local effects on tissue, Circulation 98 (1998) 290–293.
[232] R.J. Price, D.M. Skyba, S. Kaul, T.C. Skalak, Delivery of colloidal particles and red blood cells to tissue through microvessel ruptures created by targeted microbubble destruction with ultrasound, Circulation 98 (1998) 1264–1267.